HHS Public Access

Author manuscript

Inhal Toxicol. Author manuscript; available in PMC 2015 November 30.

Published in final edited form as:

Inhal Toxicol. 2012 October ; 24(12): 798–820. doi:10.3109/08958378.2012.720741.

Multi-walled carbon nanotubes: sampling criteria and aerosol characterization

Bean T. Chen, **Diane Schwegler-Berry**, **Walter McKinney**, **Samuel Stone**, **Jared L. Cumpston**, **Sherri Friend**, **Dale W. Porter**, **Vincent Castranova**, and **David G. Frazer**

Health Effects Laboratory Division, National Institute for Occupational Safety and Health, Centers for Disease Control and Prevention, Morgantown, WV, USA

Abstract

This study intends to develop protocols for sampling and characterizing multi-walled carbon nanotube (MWCNT) aerosols in workplaces or during inhalation studies. Manufactured dry powder containing MWCNT's, combined with soot and metal catalysts, form complex morphologies and diverse shapes. The aerosols, examined in this study, were produced using an acoustical generator. Representative samples were collected from an exposure chamber using filters and a cascade impactor for microscopic and gravimetric analyses. Results from filters showed that a density of 0.008–0.10 particles per μm^2 filter surface provided adequate samples for particle counting and sizing. Microscopic counting indicated that MWCNT's, resuspended at a concentration of 10 mg/m^3, contained 2.7×10^4 particles/cm^3. Each particle structure contained an average of 18 nanotubes, resulting in a total of 4.9×10^5 nanotubes/cm^3. In addition, fibrous particles within the aerosol had a count median length of 3.04 μm and a width of 100.3 nm, while the isometric particles had a count median diameter of 0.90 μm. A combination of impactor and microscopic measurements established that the mass median aerodynamic diameter of the mixture was 1.5 μm. It was also determined that the mean effective density of well-defined isometric particles was between 0.71 and 0.88 g/cm^3, and the mean shape factor of individual nanotubes was between 1.94 and 2.71. The information obtained from this study can be used for designing animal inhalation exposure studies and adopted as guidance for sampling and characterizing MWCNT aerosols in workplaces. The measurement scheme should be relevant for any carbon nanotube aerosol.

Keywords

Multi-walled carbon nanotubes; engineered nanoparticles; characterization; inhalation studies; exposure assessment method

Address for Correspondence: Bean T. Chen, Ph.D., Pathology and Physiology Research Branch, Mailstop L-2015, NIOSH-CDC, 1095 Willowdale Road, Morgantown, WV 26505-2888, USA. Fax: +1 304 285-5938. bdc4@cdc.gov.

Declaration of interest

The findings and conclusions in this report are those of the authors and do not necessarily represent the views of the National Institute for Occupational Safety and Health. The mention of any company names or products does not imply an endorsement by NIOSH, nor does it imply that alternative products are unavailable, or unable to be substituted after appropriate evaluation. The authors report no conflicts of interest. The authors alone are responsible for the content and writing of the paper.

Introduction

Since first reported by Iijima (1991), efforts in synthesis, characterization, and theoretical investigation of carbon nanotubes (CNT's) have grown exponentially. This is mainly a result of their perceived novel properties and their tremendous potential for future technological applications. Although CNT's come in a variety of forms, single-walled carbon nanotubes (SMCNT's) and multi-walled carbon nanotubes (MWCNT's) are currently the predominant structures being studied. Different from the SWCNT's which contain only one graphene layer rolled into a tube, MWCNT's consist of many coaxial layers of cylindrically arranged graphene sheets with a nanoscale diameter between 1 and 100 nm. The unique properties (e.g. large surface area, high physical strength/stiffness and exceptional electrical/thermal conductivities) and widespread applications (e.g. medical products, electronic devices, automotive and aerospace industries) of MWCNT's have led to their increased production and use (Endo et al., 2008). At the same time, however, concerns have been raised about the potential for human exposure during their use and the possible health risks they may pose (Donaldson et al., 2006). This is partly a result of the physical resemblance of MWCNT's to asbestos and other pathogenic fibers, which have toxicity associated with their morphology. Several different MWCNT inhalation studies have been performed and have reported that adverse pulmonary, cardiovascular, and immune reactions may result from exposure to MWCNT's (Li et al. 2007; Mitchell et al., 2007; Ma-Hock et al., 2009; Ryman-Rasmussen et al., 2009; Pauluhn, 2010; Stapleton et al., 2012; Porter et al., 2012). At the present time, however, very little is known about occupational exposures to MWCNT's and their potential adverse health effects.

A recent study reports MWCNT-containing airborne dust concentrations, ranging from undetectable to 440 μg/m^3 in a research laboratory during their production (Han et al., 2008). Although the mass concentration reported in this study was not composed entirely of fiber-like MWCNT's, and was significantly reduced after control measures were implemented, this study clearly indicated that airborne fiber-like MWCNT particles were present in this workplace and that inhalation exposures to airborne MWCNT's are possible and could be a major occupational hazard during manufacture, handling, and the cleanup of engineered nanomaterials. More importantly, with the growing industrial production of MWCNT's and use of CNT products, there will be a much greater potential for aerosol release on a larger scale. In response to this concern, the National Institute for Occupational Safety and Health (NIOSH) has developed an aerosol generation and exposure system (McKinney et al., 2009) to conduct toxicological investigations and risk assessment of manufactured MWCNT particles (Porter et al., 2010, 2012). Since animal studies that lack adequate characterization of the "as administered" nanoparticles (Oberdörster et al., 2005) may not provide meaningful data or conclusions for exposure and risk assessments (Warheit, 2008), both aerosol sampling procedures and particle characterization techniques are important and should be carefully designed prior to performing toxicological investigations. This is especially important for manufactured nanoparticles such as MWCNT's, because many issues related to sampling and characterization have been of great interest to the researchers and need to be thoroughly addressed when conducting exposure and risk assessment. For instance, which dose metric is most appropriate for use, mass or number? In

addition, if number is used, what sampling methods and counting rules should be used? Would it be similar to fiber counting in the case of asbestos fibers? Further, how about the argument of counting individual primary nanotubes or number of agglomerates? The tendency of aerosolized MWCNT particles to form large entangled “bird’s nest”-like structures and to combine into bundled rope configurations makes particle counting difficult, if not impossible, to perform.

The focus of this study was to establish sampling methods to collect representative MWCNT samples from an exposure chamber (“as administered”) and to develop measurement schemes to physically characterize the particles in the sample. Those sampling and characterization methods included using: (1) filters for gravimetric measurements, microscopic counting, and geometrically sizing of the particles, and (2) cascade impactors for collecting size-classified samples to determine the aerodynamic size distribution. The approaches and results documented in the report will help establish guidelines of how to sample and characterize MWCNT aerosols in a workplace or during an inhalation study. It is believed that the measurement scheme can also be used for SWCNT’s and is relevant to other CNT aerosols.

Materials and methods

MWCNT’s

CNT’s vary significantly in diameter and length depending on the manufacturing process. The diameters of CNT’s are controlled by the sizes of the metal nanoparticles (catalyst) from which they are grown. Measurements indicate that MWCNT’s generally range between 10 and 200 nm in diameter (Hou et al., 2003). Their lengths are generally dependent on the synthesis time but are typically tens of microns, although significantly shorter and longer nanotubes have been made (Motta et al., 2005).

The MWCNT bulk material used in this study was provided by Mitsui & Co. (MWNT-7, lot 061220-31; Ibaraki, Japan). The nanotubes were catalytically grown by the chemical vapor deposition process. The manufactured nanomaterial is conductive and contains fiber-like particles. According to the vendor’s information, the specific surface area of the material is in the order of 24–28 m^2/g and the particle material density is approximately 2.1 g/cm^3. This is in good agreement with measured values in our laboratory of 22.3 ± 2.1 m^2/g and 2.41 ± 0.03 g/cm^3 using the gas adsorption BET method (NOVA 2000e surface area analyzer, Quantachrome Corp, Boynton Beach, FL) (ASTM 2010a) and gas pycnometry (Micromeritics Accupyc II 1340, Norcross, GA) (ASTM 2010b), respectively.

Even though the information on this particular MWCNT lot was limited, the vendor indicated that the manufacturing parameters used in this MWCNT lot were identical to those used in a previous lot (05072001K28) in which the bulk material was characterized in detail (chemical composition, crystalline structure, metal catalyst contamination, zeta potential, length and width, etc.) by Porter et al. (2010). In that study, MWCNT samples were prepared in dispersion medium and individual nanotubes were examined after drying. High resolution transmission electron microscopic (HR-TEM) images displayed the distinctive crystalline structure of MWCNT’s with multiple numbers of graphene layers. The results

showed that the individual nanotubes had a width between 20 and 90 nm and a length up to several micrometers. These data provided the framework for describing the size dimensions and range of individual nanotubes in the MWCNT aerosol samples used in the present study.

The HR-TEM images were also used for determining the detailed internal dimensions of a MWCNT, including the width of the inner hollow core, the width of each graphene layer, and the width between two graphene sheets. This information was necessary for approximating particle mass to particle number and thus converting mass concentration to number concentration. Details of the method of estimating particle number from mass measurements are described in Appendix A. Results of those calculations show that the estimate of the number concentration was 8.0×10^3 particles/cm^3 for a mass concentration of 1 mg/m^3 (assuming an average value of 10 nanotubes per particle). It should be noted that this estimation was based on measurements of nanotubes dispersed in a liquid sample and could be different for MWCNT's dispersed as an aerosol. Nonetheless, it would serve as the first approximation to the conversion factor prior to any actual counting and gravimetric measurement of particles on a filter. In addition, the number concentration of the MWCNT aerosol depends upon how agglomerated the nanotubes were, which is represented by the mean number of nanotubes per particle (or particle structure). The calculations assumed that there was an average of 10 nanotubes per particle (or particle structure).

Generation of the MWCNT aerosol using an acoustic dispersion system

Technically, the dispersion of CNT's is difficult either in a liquid or as a dry powder. The nanotubes are hydrophobic and tend to either agglomerate yielding large entangled "bird's nest"-like structures (Figure 1A) in a non-dispersed bulk material or to bundle together in ropes (Figure 1B). The different configurations are a consequence of attractive van der Waals forces between nanotubes during dispersion. Bundles typically contain many tens of nanotubes and can be considerably longer and wider than the individual nanotubes from which they are formed. This could have important toxicological consequences, since the conventional perception is that animals are exposed to individual particles rather than agglomerates.

In the past, much effort has been made in selecting an effective dispersion medium for *in vivo* CNT studies via intratracheal instillation or pharyngeal aspiration (Sager et al., 2007; Mercer et al., 2008; Wang et al., 2010). Similarly, inhalation exposures to aerosols containing CNT's have focused on removing clumps or breaking apart large agglomerates to achieve respirable sized aerosol particles using techniques including a knife mill, a settling chamber, and cyclones (Mitchell et al., 2007; Baron et al., 2008). In this study, a dry powder dispersion technique was employed, since inhalation exposures more closely mimic occupational and environmental settings than either exposure via pharyngeal aspiration or intratracheal instillation of CNT's in a hydrosol form. In addition, rather than removing clumps or breaking apart large agglomerates within the aerosol, a simpler approach was used that allowed a gentle dispersion of particles to simulate aerosols formed during manufacturing, handling, and cleaning operations in a production plant. The aim was to use a generation system that provides aerosols with a particle size distribution and morphology similar to those found in the workplace.

An acoustical particle generation system (Figure 2A) was used to disperse a MWCNT aerosol that was in the respirable size range and suitable for animal inhalation exposure studies (McKinney et al., 2009). As shown in Figure 2A, acoustical energy generated by a speaker vibrates the top and bottom diaphragms of the generator in addition to the air column in the cylinder. The energy displaces the bulk material releasing particles and suspending them in the air. The constant air through the chamber generates a flow pattern resembling that of a vertical elutriator and prevents coarse particles and large agglomerates from leaving the chamber. The aerosol containing the respirable particles is then introduced into an exposure chamber. In order to optimize the aerosol stability in the chamber, a feedback control system, containing electrical and mechanical hardware along with computer software, was used to maintain the desired, tightly controlled, aerosol concentration in the chamber. Scanning electron microscopic (SEM) images of MWCNT aerosols generated with this system were previously shown by McKinney et al. (2009). They were similar to those found in a MWCNT manufacturing plant (Han et al., 2008) and, as a result, the generated aerosol appears to be representative of real world exposures and well suited for inhalation toxicological investigations. In this study, particle characterization was conducted with a target concentration of 10 mg/m^3 in a chamber that was later used for animal inhalation studies (Stapleton et al., 2012; Porter et al., 2012). The mass concentration was continuously monitored using a Data RAM (DR-40000 Thermo Electron Co, Franklin, MA).

Sampling methods

Since airborne nanomaterials often consist of mixtures of individual nano-sized particles as well as micron-sized agglomerates with complex structures and irregular shapes, conventional sampling approaches were primarily used to evaluate aerosol characteristics including: (1) collecting filter samples for number and mass concentrations, geometric size, and morphology, and (2) using a cascade impactor to acquire size classified samples for aerodynamic size distribution and other analyses. Commercially available near-real-time instruments that typically measure a specific physical property of a spherical aerosol particle (e.g., electrical mobility, light scattering, etc.) and relate that property to the particle size for instrument calibration may not always be appropriate for use in evaluating aerosol characteristics of manufactured nanomaterials such as MWCNT's. In this study, however, they were used for comparison measurements. In most cases, at least three samples were used to provide the needed accuracy.

PTFE filter samples for mass concentration

The average concentration in the chamber was determined gravimetrically by taking two 37-mm polytetrafluoroethylene filter (PTFE, 0.45 μm pore size, SKC Inc., Eighty Four, PA) samples at a flow rate of 0.5 L/min for 5 h. The mass concentrations were calculated from the change in weight of the filter, airflow rate through the filter, and the sampling time. A balance (Mettler-Toledo, Model UMX2, Columbus, OH) with a resolution of 0.1 μg was used to measure filter weights. These data were routinely used to calibrate the Data RAM.

Polycarbonate filter samples for number-based concentration and size distribution

Sample preparation and collection—Since the morphologic features (e.g. high aspect ratio) of the fiber-like particles in MWCNT aerosols are similar to those of asbestos fibers, the NIOSH standard 7402 (NIOSH, 1994a) measurement method using membrane filters and microscopic analysis was initially adopted as a guideline for quantitatively describing MWCNT aerosols. However, modifications to the method, such as the selection of filter and defining the optimal range of particle number on filter surface (surface density), were necessary to optimize the technique for use with MWCNT's. Details of the sampling method development for microscopic observations of MWCNT's particles are described in Appendix B.

In brief, a 25-mm polycarbonate filter of 0.1 μm pore size (Whatman, Clinton, PA) was mounted in a closed-face filter holder with a 5-cm electrically conductive plastic extension cowl. This filter assembly was used for collecting MWCNT samples from the exposure chamber. Due to the high pressure drop across the filter, the sampling flow rate was fixed at 0.4 L/min. A series of sampling time intervals between 5 s and 2 min was used for the initial trials. These values were selected based on the optimal surface density of 0.008–0.10 particles/μm^2 (proposed in Appendix B) with the known mass concentration, filter area (=420 mm^2), flow rate, and the approximate conversion factor between mass and number concentration (see Appendix A).

After sampling, a slight vacuum was applied downstream of the holder to insure that MWCNT particles in the sample were collected on the filter, not attached to the internal surface of the inlet or extension cowl of the filter holder. The sample was then analyzed using a field emission scanning electron microscope (FE-SEM; Hitachi, S-4800, Tokyo, Japan).

Differentiation of fiber-like and isometric particles—As described in Appendix B, there are many different configurations of particles in an MWCNT aerosol sample (Figure 1C). Although the sampling flow and time provided an optimal density of particles to be counted on the filter, the complexity in nanotube agglomeration and the diversity of particulate morphology made optically particle sizing difficult (Figure 1E). The sample appears to contain particles of many different shape configurations including single smooth nanotubes with various aspect ratios (L/W, *L*, length and *W*, width or diameter), bundled nanotubes, nanotube nodules (fiber-like particles having nano-sized nodules attached), and isometric-shape or fiber-like agglomerates having nanotubes and/or compact particles attached. While the "individual nanotubes" are easy to identify as fiber-like particles that contain mainly elemental carbon, the agglomerates ("CNT structures") could consist of nanotubes, nodules, and/or compact particles with heterogeneous compositions. Since fiber-like particles and isometric-shape particles have different aerodynamic behaviors in the air stream and distinct deposition patterns in the respiratory tract, a practical approach in performing particle size analysis would be to visually separate the MWCNT particles into two categories, fiber-like (fibrous) particles and isometric particles (Figure 1F). The size and number of the particles in each category could then be determined.

Particles that had a shape for which the dimensions were approximately the same in all directions were classified as isometric particles, while particles with an aspect ratio (L/W) of 3 or greater in two dimensions were defined as fibers in the NIOSH standard 7400 (NIOSH, 1994b). This approach, combined with an appropriate magnification of FE-SEM micrographs, allowed particles in each category to be differentiated, counted and sized. It should be noted that this differentiation is solely based on physical structure, not on chemical composition, of the aerosol particles, since the physical characteristics affect their aerodynamic behavior in the air stream and deposition dosimetry in the respiratory tract.

Counting and sizing particles using FE-SEM—Conventional microscopic observations of particles deposited on a filter were used to provide direct measurements of the MWCNT particle sizes and number concentrations. Particle counting and sizing were conducted simultaneously by selecting the proper FE-SEM magnification in a representative area of the filter surface. Since the particles covered a wide size range in terms of their lengths and widths (as indicated in Appendix B), both low and high magnifications between ×2K and ×40K were used so that all particles could be differentiated, counted, and sized. Fields of view over the entire effective sample area, including edge regions, were randomly selected for each filter. Approximately 500–600 particles were examined on each filter sample.

Counting was used to determine the total number concentration of particles on a filter along with the number concentration of fibrous and isometric particles. During the counting process, the number of primary components (including individual nanotubes of various aspect ratios, nano-sized nodules, and/or micron-sized compact particles) in each particle structure was computed. The numbers of nanotubes were often difficult to count in heavily agglomerated samples, so their numbers were estimated based on the cross-sectional area of the agglomerate and the average area of slightly agglomerated particles whose nanotubes could be counted. This method was used more often for isometric particles because most heavily agglomerated particles appeared to be more isometric in overall shape. Since the components in the MWCNT particles were found to contain primarily nanotubes (Porter et al., 2010), the term “numbers of nanotubes per particle (NNP)” is used throughout this report to represent the number of primary components in a particle structure, and its mean value is used as an index to express the degree of agglomeration in the test aerosol.

The geometric equivalent diameter was used for sizing isometric particles. It was defined as the diameter of a sphere that has the same compact geometry as the particle (including internal voids), similar to the projected area diameter when a transmission electron microscopic image was used. Even though isometric particles were found mainly in agglomerates containing voids, both inside and between nanotubes, an equivalent diameter was chosen because the measurement was simple and practical for microscopic analysis. The number of isometric particles in selected size intervals was used to characterize the particle size distribution and to assess if the size distribution could be described by lognormal statistics.

In order to size fibrous particles, both the length and width of each particle were measured to determine if each dimension followed a lognormal distribution. The distributions of particle

lengths and widths were correlated to determine if they could be described by a joint bivariate lognormal distribution. This approach was used previously to describe airborne man-made mineral fibers (Schneider et al., 1983) and asbestos fibers (Cheng, 1986). The detailed procedures for characterizing fibrous particles, described by Cheng (1986), were followed in this study.

Cascade impactor samples for mass-based aerodynamic size distribution and size-fractionated microscopic analysis

Preparation and collection of foil, filter, and grid samples—Two Micro-orifice Uniform Deposit Impactors (Model MOUDI-110 and Nano-MOUDI-115, MSP Corp., Shoreview, MN) were used in tandem to collect aerodynamic size-classified samples of the total MWCNT aerosol from the animal exposure chamber. The unique micro-orifice design of the MOUDI accomplishes size segregation of particles without the necessity of using very low pressures in the lower stages. This design enables the collection of size-segregated samples of particles from 18 μm (cutoff diameter of the 1st stage) down to 10 nm (cutoff diameter of the 14th stage). The total flow rate through the impactor was 30 L/min, but dilution air was added so only 5 L/min were drawn from the chamber to minimize potential airflow disturbances that influence the concentration and homogeneity of the aerosol in the chamber.

Special procedures for sample preparation and operating the MOUDI were followed, while simultaneously collecting size-segregated samples for microscopic counting, sizing, and gravimetric measurements. Two different collection mediums were prepared for the first 14 stage substrates of the impactor: (1) 47-mm aluminum foils for gravimetric measurements, and (2) polycarbonate filters with electron microscopic grids attached at their center for particle morphology analysis. A backup filter was used on the final stage. The aluminum foil substrates were pre-coated with silicon oil to avoid particle bounce from an upper stage that would contaminate a sample collected on a lower stage. The polycarbonate filters were sputter-coated with a thin layer of gold/palladium (SPI-Module, Structure Probe Inc., West Chester, PA) for 20 s at 20 mA to avoid undesired deposits on the sample due to electrostatic forces. A complete set of 14 foils, 14 filters (with grids), and a backup filter were prepared for each sample period, and the foils and the backup filter pre-weighed. Since the filters and grids were used for microscopic observations and were not sprayed with silicon oil, an aluminum foil covered with silicon oil spray was placed on the preceding stage to eliminate particle bounce from that stage. With this conceptual design, the following procedures were followed:

1. A half set of the oil-coated foils (7) and a half set of the filters/grids (7) were placed on alternate stages of the MOUDI in addition to a backup filter on the final stage.
2. Different sample time intervals between 0.5 and 4 min were used to provide an optimal range of particle surface density on each filter stage
3. After sampling, the seven foils and seven filters with grids were removed from the impactor stages.

4. The MOUDI was reloaded with the second half of the oil-coated foils and filters/grids, but the foils were replaced with filters and the filters with foils.
5. The same sample periods were used as before.
6. A complete set of 14 filter/grid samples were assembled for microscopic analysis.
7. The complete set of oil-coated foil samples were placed in the impactor for another 30 min sample period. [Note: the longer sampling time was to ensure the collection of sufficient mass for gravimetric measurements].
8. The 14 foil samples were removed from the impactor along with the backup filter and reweighed for a gravimetric analysis.

Analysis of size-classified samples—At the end of each sample period, the complete set of 14 foil samples and the backup filter were gravimetrically measured, and the mass-weighted particle size distribution was determined using a data inversion method (O'Shaughnessy & Raabe, 2003). While filter samples were prepared as previously described (in the subsection of "Sample Preparation and Collection" and Appendix B) and the particles were viewed using the FE-SEM (Hitachi), the microscopic grids were detached from the filters and the particles were directly viewed using a JEOL 1220 transmission electron microscope (TEM, JEOL Inc, Toyko, Japan). Using the FE-SEM micrographs, the number of particles on each filter stage was examined to estimate the stage with the greatest number of particles. The combined results from gravimetric measurements and the FE-SEM micrographs were used to qualitatively estimate both the mass mode and count mode of the overall particle size distribution. In addition, the aerodynamic size classified grid samples were examined with the TEM to differentiate between the number of fibrous and isometric particles on each stage. Microscopically determined equivalent diameters of individual particles with well-defined shapes were compared with the aerodynamic diameters of particles on the corresponding stage to determine the effective particle density for isometric particles and the dynamic shape factor for fibrous particles. Well-defined isometric particles were those particles having a relatively compact structure and an aspect ratio less than or equal to 1.5, while well-defined fibrous particles were those composed of individual nanotubes. To avoid examinations of complex structures, only well-defined particles were selected from grid samples for TEM examination and future analysis.

Determination of effective particle density for well-defined isometric particles —The effective density, ρ_p, for a well-defined isometric particle on the i-th stage of the MOUDI can be expressed as:

$$\rho_p = [d_{ae}{}^2 \rho_o C(d_{ae})] / [d_{pa}{}^2 C(d_{pa})] \quad (1)$$

In this expression, $d_{ae} = (d_{i-1} \times d_i)^{1/2}$, where d_i is the 50% cutoff diameter on i-th stage [i = 1 is the inlet stage], d_{pa} is the projected area equivalent diameter determined from the TEM photomicrograph, ρ_o is the unit density, and $C(d_{ae})$ and $C(d_{pa})$ are slip correction factors based on d_{ae} and d_{pa}, respectively. Since d_{ae} is defined based on the geometric mean of the distribution of classified particles on a given stage, the value of d_{pa} was selected based on

the geometric mean of the distribution as well. This is conventionally accepted because the size distribution of the particles segregated by a given impactor stage is considered to follow a lognormal distribution if the size of the unclassified isometric particles can be represented by a lognormal distribution (Mercer, 1963; Hinds, 1986). It is important to note that, different from the material density (without voids) and the fiber density (with voids) of a single nanotube particle [see Eq. (3) and Appendix A], the effective density refers to a well-defined isometric particle with multiple nanotubes (with voids inside and between nanotubes).

Determination of the dynamic shape factor of fibrous particles composed of individual nanotubes—According to Baron et al. (2001), the particle dynamic shape factor, κ_p, for an individual fibrous nanotube particle on the i-th stage of the MOUDI can be expressed as:

$$\kappa_p = d_m^2 \rho_m C(d_m) / [d_{ae}^2 \rho_o C(d_{ae})] = \kappa \delta C(d_m) / C(d_e) \quad (2)$$

$$\kappa = d_e^2 \rho_f C(d_e) / [d_{ae}^2 \rho_o C(d_{ae})] \text{ and } \delta = (\rho_m / \rho_f)(d_m / d_e)^2 = d_e / d_m \quad (3)$$

where d_m represents the mass equivalent diameter [$d_e (\rho_f/\rho_m)^{1/3}$] of the particle, d_e is the envelope equivalent diameter [$(3W^2L/2)^{1/3}$], ρ_m is the material density of the particle (without voids) [2.1 g/cm^3, the density of graphene], ρ_f is the fiber density of the nanotube particle (with voids) [see Appendix A], and C(d_m or d_e) is the slip correction factor based on the diameter d_m or d_e. The mass equivalent diameter represents the diameter of a nonporous sphere composed of a bulk particle material that has the same mass as the particle. The envelope equivalent diameter is the diameter of a sphere that has the same envelope and mass as the particle (including voids). When there are no voids in the particles, $d_m = d_e$ and $\kappa_p = \kappa$. Since fibrous nanotube particles contain voids between graphene sheets, the particle dynamic shape factor, κ_p consists of not only the component κ, which is the dynamic shape factor solely due to the fiber-like shape, but also a component δ, which is associated with the particle porosity and void space inside the nanotube. For practical reasons, the shape factor, κ (not κ_p), of nanotube particles was assessed using Eq. (3), since the length and width of the fiber-like particle could be microscopically determined.

Alternatively, the shape factor κ can be estimated by considering each nanotube particle as a prolate spheroid moving in the air. In this case, κ is a function of the particle's aspect ratio (β (L/W) and its orientation in air with regard to the particles major axis (Stöber, 1972) expressed as

$$\kappa_1=8(\beta^2-1)/\left[3\beta^{1/3}((2\beta^2-3)\ln(\beta+(\beta^2-1)^{1/2}))/(\beta^2-1)^{1/2}+\beta\right]\ \kappa_2=4(\beta^2-1)/\left[3\beta^{1/3}((2\beta^2-1)\ln(\beta+(\beta^2-1)^{1/2}))/(\beta^2-1)^{1/2}-\beta)\right]\ \kappa_3=3/(1/\kappa_1+2/\kappa_2) \quad (4)$$

where κ_1, κ_2, and κ_3 are dynamic shape factors of the particle with a perpendicular, parallel, and random orientation. The aerodynamic diameter, $d_{ae,j}$, of a nanotube particle according to its orientation can be calculated using the following relationship:

$$d_{ae,j}=d_e(\rho_f C(d_e)/\rho_o\kappa_j C(d_{ae}))^{1/2} \quad (5)$$

where j = 1, 2 and 3 represent perpendicular, parallel, and random orientation, respectively. The mean value of $d_{ae,j}$ calculated for nanotube particles with different orientations in air (κ_1, κ_2, and κ_3) can be compared with $d_{ae} = (d_{i-1} \times d_i)^{1/2}$, which is based on the 50% cutoff diameter of compact spheres on a given impactor stage. The cut-off diameter for spheres of the i^{th} stage is d_i, and d_{i-1} is the cut-off diameter of the previous stage. The mean κ_j value whose $d_{ae,j}$ is closest to d_{ae} represents the shape factor of nanotube particles having the most probable orientation in air. Calculations, along with TEM photomicrographs of particles collected on a particular impactor stage, can be used to evaluate the performance of the impactor in separating different sized fibers that have an assumed orientation.

It is important to emphasize, once again, that only those individual nanotubes with well-defined width and length were selected for characterization of their dynamic shape factor κ. This is because it is difficult, if not impossible, to predict the behavior and collection efficiency of MWCNT aerosol particles with complex configurations and high aspect ratios (see Figure 1C). Note that, in an impactor, even simple fiber-like particles are difficult to model because they experience a periodic instability under a coupled motion of translation and rotation, and perform a “flip” in rapidly changing flow conditions (Gallily et al., 1986; Asgharian et al., 1997).

Aerosol measurements using two near-real-time instruments

Two near-real-time instruments, an electrical low pressure impactor (ELPI, DEKATI, Tampere, Finland) and a scanning mobility particle sizer (SMPS Model 3936; TSI, Inc.), were used to investigate MWCNT aerosols. Measurements made with these instruments were compared with conventional methods using a MOUDI and gravimetric analysis. The ELPI combines unipolar corona charging and aerodynamic size classification of the particles along with the electrical detection of the charged particles. The SMPS measurements are based on bipolar ion charging and the differential electrical mobility of particles, which are size separated and counted with a condensation particle counter. Both instruments are

frequently used for determining size distributions of ultrafine particles in the ambient and occupational environments because they operate in near-real-time.

Results

Aerosol generation system performance: stable mass concentration of test aerosol

Figure 2 shows (A) the schematic diagram of the aerosol generation system, (B) the calibration results illustrating a linear relationship between Data RAM readings (an integration time of 2 second) and concentration data (3–12 mg/m^3) derived from gravimetric measurements, and (C) a representative profile of the Data RAM readings and speaker voltage outputs during a 5-h exposure at a target concentration of 10 mg/m^3. The variability of the aerosol concentration during any given day was less than 2%, and the day-to-day variation was less than 5% for periods as long as 4 weeks.

Number concentration

Images of MWCNT particles collected on polycarbonate filters with a pore size of 0.1 μm were analyzed using the FE-SEM under several different magnifications. First, photographs (similar to those shown in Figures 1E–1G) were used to determine if particles were either fibrous or isometric in shape. Then the same photos were used to estimate particle size and to determine the value of the NNP. Using the procedures described in the Methods section, 500–600 particles were examined in a total area of 3.0–4.0 × 10^4 μm^2 on a polycarbonate filter where there were between 0.015 and 0.017 particles/μm^2, which is within the range of 0.008–0.1 particles/μm^2 proposed in Appendix B.

The number concentration was estimated to be between 2.1 and 3.8 × 10^4 particles/cm^3 with an average of 2.7 × 10^4 particles/cm^3. Each particle consisted of a NNP value between 14 and 23. Among the samples analyzed, approximately 20–40% of the particles were classified as isometric particles and the remaining 60–80% were classified as fibrous particles. Figure 3 shows the distribution as a histogram of the NNP in a representative sample of the aerosol. The distribution follows lognormal statistics, and the median value was estimated to be 16 with a geometric standard deviation (GSD) of 2.1 (Figure 3A). The fibrous fraction of the aerosol had a relatively uniform distribution within the interval between 1 and 20 nanotubes per particle with a mean of 16 nanotubes per particle (Figure 3B). The isometric particles maintained a left-skewed distribution with a mean of 30 nanotubes per particle and more than 60% of them contained more than 20 nanotubes (Figure 3C). The magnitudes of the histograms in Figures 3A–3C are expressed as a fraction normalized with respect to the number of nanotubes per particle.

Among all the samples, 3–5% of the particles (or particle structures) counted were individual particles, 35–50% of them contained less than 10 nanotubes, and only 6–10% contained more than 30 nanotubes. An average value of 18 nanotubes per particle was estimated for the overall MWCNT particles by using the NNP values between 14 and 23.

Particle geometric size distribution

The FE-SEM images of the filter samples were used to categorize and size both the fibrous and isometric particles. The length and width of fibrous particles were measured individually, while only the geometric equivalent diameter was measured for isometric particles. Table 1 shows the measured dimensions of fibrous particles from a representative sample presented in a length-width matrix. Similar information is presented in Figure 4A to illustrate the count- or number-based size distribution of the fibrous particles characterized in terms of their length and width. The particle width ranged from 15 nm to greater than 500 nm and particle length varied between 0.2 μm and greater than 15 μm. The particle aspect ratios assumed values between 4 and 200 (Figure 4B). The distribution of the aspect ratios of the fibrous particles had a geometric mean of 31.0 and a geometric standard deviation of 2.09.

Assuming the samples of fibrous particles were taken from a bivariate lognormally-distributed population, the mean and variance of the natural logarithm of length (L) and width (W) were estimated along with the correlation factor between In L and In W. Following the procedures described by Cheng (1986), the count median fiber width (CMW) was calculated to be 100.3 nm with a geometric standard deviation (GSD_W) of 1.73, and the count median fiber length (CML) was 3.04 μm with a geometric standard deviation (GSD_L) of 2.23. The correlation factor (τ) between L and W was 0.47. Based on these five parameters, the probability density function (F_{LW}) for the sample was determined and plotted in Figure 4C. The hypothesis that the sample of fibrous particles was taken from a bivariate lognormally-distributed population was found to be valid using the chi-square test of the deviation of the data from the theoretical expectations.

The range of the geometric equivalent diameters was between 0.1 and 5.6 μm for isometric particles samples. The histogram of geometric equivalent diameters (Figure 5) shows the percent number concentration per unit size interval (N = number concentration, D_G = geometric equivalent diameter). The distribution can be represented with a lognormal relationship having a count median diameter (CMD_G) of 0.90 μm and a GSD of 2.08.

Particle aerodynamic size distribution

Aluminum foil substrates and filters with microscopic grids obtained from the MOUDI cascade impactor were used to determine the mass- and number-based particle size distribution based on the aerodynamic behavior of MWCNT particles. Figure 6 shows a typical size distribution of MWCNT particles found using the gravimetric measurements of foil samples from the impactor (M = mass concentration and D_{ae} = aerodynamic diameter). The histogram shows the percent of mass concentration per unit size interval. Assuming that the distribution follows lognormal statistics, it has a mass median aerodynamic diameter (MMAD) of 1.49–1.51 μm and a GSD of 1.65–1.70 (O'Shaughnessy & Raabe, 2003). Visual inspection of the filter and grid samples under the field emission scanning and the transmission electron microscopes qualitatively indicated the number-based distribution had a peak on the 8th stage [count mode = 0.42 μm], while the aluminum foil samples showed gravimetrically that the mass-based size distribution had a peak on the 6th stage [mass mode

= 1.34 μm]. Note that the information presented here applied to all the particles in MWCNT aerosol, including both fibrous and isometric fractions.

Microscopic measurements of size-classified particles

In addition to the foil and filter samples used for aerodynamic size analysis, corresponding grid samples collected on filters obtained from the MOUDI were further examined. The MWCNT particles deposited on these samples were viewed using a JEOL 1220 TEM. Figure 7A–7F illustrates examples of TEM photomicrographs of particles collected on stages 6–11 of the MOUDI with their measurement details given in Table 2. Note that only stages containing well-defined particles were selected for TEM examination of the particles and further analysis.

Table 2 shows the 50% cutoff diameter of the impactor stage, the particle count, and the mean and standard deviation of the particle distributions on the matching grid. N_p represents the number of particles counted from an equivalent area on each grid. The results show that samples taken from the upper stages (e.g. 6^{th} and 7^{th} stages) tend to have similar numbers of well-defined isometric and fibrous particles, whereas samples on the lower stages (e.g. 10^{th} and 11^{th}) contain more fibrous particles than isometric particles. In addition, the greatest number of isometric particles were collected on the 8^{th} stage [N_p = 44], whereas the greatest number of fibrous particles were collected on the 9^{th} stage [N_p = 69].

The images (Figure 7A–7F) illustrate a decreasing trend in physical size of the particles as the impactor stage number increased from 6 to 11. This trend was substantiated in Table 2 which demonstrates that the mean projected area diameter, d_{pa}, decreased from 1.46 to 0.15 μm for isometric particles and the mean values of length and width (L, W) of the fibrous particles decreased from (6.38 μm, 206 nm) to (1.38 μm, 52 nm). The results also indicate that there were significant variations in the measurements, as evidenced by the relatively large standard deviations (SD) with respect to the means.

Determination of effective particle density for isometric particles and dynamic shape factor for fibrous particles

The density of well-defined isometric particles can be estimated after their mass and projected areas have been determined. Table 2 gives the effective particle density of the isometric particles, ρ_p that was calculated using Eq. (1). The density varied from 0.50 to 0.88 g/cm^3 between impactor stages without showing a specific trend.

The dynamic shape factor, κ, of well-defined fibrous particles was determined using two different approaches. The first was with an indirect method using Eq. (3) and assuming that the 50% cutoff diameters of compact spheres on the stages also applies to MWCNT fibrous particles. The second approach used Eq. (4) and assumed that the nanotube could be modeled as a prolate spheroid moving in the air in one of three orientations. In Table 2, the dynamic shape factors found using the first approach varied between stages. It decreased monotonically from 2.50 for the particles on the 11^{th} stage to less than unity for the particles on the 6^{th} stage. Using the second approach, the calculated values of κ were less variable, ranging from 1.94 to 2.71 between stages. In addition, it was determined that assuming

parallel orientation of the particles in all the stages except the 11th gave the best results. The particles on the 11th stage appeared to be modeled best by assuming they were oriented randomly.

Measurements using ELPI and SMPS

Figure 8 shows the representative number-based size distributions of the MWCNT aerosol obtained from both the ELPI and SMPS. The ELPI measurements indicate a particle size distribution with a count median diameter of 450 nm (count mode = 0.43 μm) with a GSD of 2.09. The number concentration was 3.3×10^4 particles/cm^3.

Although the SMPS cannot be used to detect particles greater than 0.65 μm, the complete size distribution of the MWCNT aerosol can be estimated by assuming that the particle size distribution followed unimodal lognormal statistics. Based on this presupposition, the SMPS indicated a size distribution having a count median of 360 nm (count mode = 0.35 μm) and a GSD of 1.70. The total number concentration was 4.2×10^4 particles/cm^3 which was 27% greater than the ELPI measurement.

Discussion

In this study, the aerosol generator developed by McKinney et al. (2009) was used to deliver tightly controlled concentrations of MWCNT aerosols with a mean ± standard deviation of 10.02 ± 0.19 mg/m^3 and a daily range between 9.4 and 10.5 mg/m^3. The particle morphologies appear to be similar to those found in the workplace (Han et al., 2008). Sampling criteria and procedures were developed to collect desirable samples produced by the generation system for particle characterization. Aerosol samples were described in terms of particle number, number concentration, and particle mass concentration. Based on the physical shape, particles were classified as either fibrous or isometric. The two classes were characterized first individually and then in a combined state, and the degree of particle agglomeration within each form was determined. In addition, the effective density of the simple isometric particles and the shape factor of the individual fibrous nanotubes were calculated.

Aerosol sampling criteria

Using an approach similar to NIOSH standard 7402 for counting asbestos fibers, a particle surface density of 0.008–0.10 particles/μm^2 was proposed as a reasonable range of deposition for microscopic observation of MWCNT particles on 25-mm polycarbonate filters with 0.1-μm pore sizes. The results indicated that filters with a surface deposit between 0.015 and 0.017 particles/μm^2 (within the proposed range) did provide suitable samples (Figure 1E–1G) for microscopic measurements, demonstrating that this range can be recommended.

The advantage of determining the optimal range of particle surface density on a sample filter is that it can be used to determine the appropriate sampling flow rate, Q, and the time, *T*, needed for an adequate sample using Eq. (6),

$$Q \times T = \text{Surface density} \times \frac{\text{surface area}}{\text{Number concentration}} \quad (6)$$

Surface area, in this expression, is the effective sample area on the filter surface for aerosol collection and can be measured from the distinctive circular deposit of MWCNT particles on the filter (e.g. approximately 420 mm^2 on our 25-mm filter samples). As an example, assume that an optimal density of 0.02 particles/μm^2 was selected for sampling the aerosol in a chamber that has a total MWCNT concentration of 10 mg/m^3 or an equivalent of 2.7×10^4 particles/cm^3 based on the mass to number conversion. A 47-sec sample collected at a flow rate of 0.4 L/min would be required to obtain a satisfactory 25-mm filter sample for particle counting and sizing analyses.

In the field, it is usually more practical to use particle mass rather than particle number to describe the concentration of the collected aerosol sample. Since 10 mg/m^3 is equivalent to 2.7×10^4 particles/cm^3 for the MWCNT sample (i.e. 1 μg ≈ 2.7×10^6 particles), the guideline of having a particle surface density of 0.02 particles/μm^2 would apply to a mass surface density of 7.4×10^{-3} μg/mm^2. This requires a mass deposit of 3.1 μg on a 25-mm filter to have an adequate sample for characterization. Since detecting such a tiny amount of sample weight could be a concern, an alternative would be to use a larger filter (e.g. 37-mm or 47-mm) and to accept a higher surface density guideline (e.g. 0.05 particles/μm^2) to have a sufficient mass for detection. Now, consider a test environment having a total MWCNT concentration of 44 μg/m^3. This is approximately 10% of the peak aerosol concentration previously reported in a research laboratory (Han et al., 2008). The time required to achieve a detectable surface density of 0.05 particles/μm^2 [or 7.8 μg on a 25-mm filter] would be approximately 7.4 h at a flow rate of 0.4 L/min. A typical field sample collected during an 8-h work shift, at this concentration, would provide a detectable mass of total MWCNT's for microscopic characterization.

Number concentration vs. mass concentration

It is important to note that the term "number" represents the quantity of either particles (or particle structures) or nanotubes in the MWCNT aerosol. At a concentration of 10 mg/m^3, the mean number concentration was found to be 2.7×10^4 particles/cm^3, which was equivalent to a total of 4.9×10^5 nanotubes/cm^3 assuming a mean of 18 nanotubes per particle. This concentration is in general agreement with the estimate of 8.0×10^5 nanotubes/cm^3 that was based on the dimensions obtained from photographic images of individual multi-walled nanotubes having a mass concentration of 10 mg/m^3 (see Appendix A). The agreement between calculations was noteworthy considering there were potential discrepancies due to the size limitation of the dots in the HR-TEM image plot, the estimation of the mean number of nanotubes per particle during counting, and the assumptions made for assessing the nanotube size distribution in a dried hydrosol sample. It is also interesting to note that, although the particle concentration varied between 2.1 and 3.8 $\times 10^4$ particles/cm^3, the nanotube concentration in the MWCNT samples remained relatively consistent at about 4.9×10^5 nanotubes/cm^3. This suggests that a constant mass concentration provided a nearly constant nanotube concentration but did not necessarily

provide a constant particle number concentration of fibrous particles combined with isometric particles. The variation in the number concentration is also related to the number of nanotubes per particle which would be a function of the degree of agglomeration in the aerosol (discussed later).

Keep in mind that the relationship, between 10 mg/m^3 and 2.7 × $l0^4$ particles/cm^3, applies only to the test MWCNT aerosol generated by the acoustical dispersion system and may vary with other types of MWCNT materials (e.g. size dimensions and electrical property), the method of dispersion (powder dispersion vs. liquid nebulization or electrospraying), and the aerosol delivery system (e.g. use of dilution air, bipolar ion source, and air cyclone). For instance, it is likely that a higher mass concentration may enhance agglomeration of nanotubes and result in a higher mean value of nanotubes per particle. In other words, a mass concentration of 20 mg/m^3 could have an equivalent mean number concentration less than 5.4 × 10^4 particles/cm^3, whereas a mass concentration of 5 mg/m^3 may have an equivalent mean number concentration higher than 1.4 × 10^4 particles/cm^3.

The difference in the number concentration of “nanotubes vs. particles” is an important issue in evaluating the risk assessment of inhalation exposure to MWCNT’s, in addition to the conversion between mass and number concentration. When evaluating the inhalation toxicology of nanoparticles, there has been a trend to describe the exposure metric of aerosol particles by emphasizing their number concentration and nano-sized primary particles rather than their mass concentration and micron-sized agglomerates. This is partly because aerosol instruments with near-real-time features can provide particle number concentrations relatively quickly, whereas microscopic and gravimetric analyses of filters or size selective samples can be very time consuming. Even though there is little information on how MWCNT particles would behave in the periphery of the lung, it is apparent that their biological response may be related to the particle agglomeration and more associated with total number of nanotubes on the alveolar surface, rather than the total number of particles in the aerosol. For example, well-dispersed CNT’s with small structures have been shown to enter the interstitial compartment of the lung and induce interstitial lung fibrosis. In contrast, poorly-dispersed CNT’s with agglomerated structures deposit at the terminal bronchioles and proximal alveoli and induce granulomatous lesions (Mercer et al., 2008). Therefore, when dealing with dose-response relationship, consideration of the number of nanotubes per particle, in addition to the total number of particles, may be the most appropriate biological exposure index. This concept would apply to the MWCNT’s used in this study, as well as to other nanotubes with similar physicochemical properties.

Agglomeration

Nanotubes have a strong tendency to agglomerate and bundle together in ropes as a consequence of attractive van der Waals forces, which are analogous to the forces that bind sheets of graphene (Thess et al., 1996). Their degree of agglomeration is especially important when characterizing MWCNT particles, because it affects their size distribution as well as their number concentration. In this study, an index of the agglomeration of MWCNT’s was achieved by counting how many nanotubes were contained in each particle (NNP). Results from a representative sample illustrate that the distribution of NNP followed

a lognormal distribution (Figure 3A). Among the samples, the average number of nanotubes per particle was about 18 for the MWCNT aerosols tested.

Another intriguing issue is whether highly-agglomerated particles should be removed from aerosols generated for animal exposure studies. For instance, in some inhalation toxicological studies, exposures have been conducted after coarse particles had been removed from the aerosol with a size selective device, such as a cyclone (Baron et al., 2008). The decision depends on the purpose of the study: to deliver an aerosol with primarily individual particles for dose enhancement or an aerosol close to that occurring in workplaces. There is no doubt that agglomeration affects the particle size distribution of the aerosol, the deposition dosimetry in the respiratory tract, and the potential biological effects. Although an aerosol having more agglomerates may result in a higher deposit in the nasopharyngeal region and thus a lower dose in the alveolar region, such an aerosol may be similar to that found in the workplace so that the exposure conditions and deposited dose would be accurately simulated during animal exposures. The total MWCNT test aerosol generated in this study had a MMAD of 1.5 μm with a GSD of 1.67. More than 90% of the particles in mass were considered to be respirable. As a result, the agglomerated portion of the aerosol particles would be included in the test aerosol for animal exposure studies. The effects of agglomeration on the aerodynamic characteristics of MWCNT aerosols, however, present an interesting research subject to be studied at a later date.

Isometric particles vs. fibrous particles

Since MWCNT particles are difficult to characterize in terms of a single population, because of their diverse and complex structures, they were individually separated in this study into two fractions, fibrous particles versus isometric (nonfibrous) particles, using microscopic analyses. The two classes of particles could be readily distinguished by differences in their aspect ratio, and each class possesses different aerodynamic behaviors and penetration/deposition characteristics in the respiratory tract. The results show that the fibrous particles were more numerous (60–80 vs. 20–40%) but contained fewer nanotubes per particle than the isometric particles. This is illustrated in Figure 3B and 3C which demonstrates the fibrous particles had an average of 16 nanotubes per particle whereas 60% of the isometric particles had greater than 20 nanotubes per particle structure. The fact that isometric particles contain more individual nanotubes per particle structure than fibrous particles suggests that the MWCNT particles bind more strongly in the isometric form than in the fibrous form.

Geometric size distribution

Although the mass-based size distribution is based on the gravimetric measurements of overall particles in the size-classified MOUDI samples (discussed in the next section), the number-based size distribution requires the counting of the shape-differentiated isometric or fibrous particles in the filter samples described in the last section.

The results indicate that the geometric size distribution of the isometric particle fraction within the MWCNT aerosol can be expressed lognormally. In addition, the length and width of the fibrous particle distributions were successfully correlated using a lognormal function,

and the joint width-length distribution could be described with a bivariate lognormal distribution (Figure 4C). Based on the bivariate analysis (Cheng, 1986), other relevant properties of the fibrous particles, including their aspect ratio, volume, surface area and aerodynamic diameter, were also shown to be lognormally distributed. In addition, the results showed that the distribution of fiber aspect ratios was lognormal along with the count median aspect ratio (CMAR), and the geometric standard deviation (GSD_{AR}). The CMAR and GSD_{AR} were expressed as:

$$\mathrm{CMAR}=\mathrm{CML}/\mathrm{CMW}\ \mathrm{GSD}_{\mathrm{AR}}=\exp[\ln^2\mathrm{GSD}_{\mathrm{W}}+\ln^2\mathrm{GSD}_{\mathrm{L}}-2\tau(\ln\ \mathrm{GSD}_{\mathrm{W}})(\ln\ \mathrm{GSD}_{\mathrm{L}})]^{1/2} \quad (7)$$

The calculated values of the CMAR and GSD_{AR} were 30.3 and 2.08, respectively, which are in good agreement with the median of 31.0 and the geometric standard deviation of 2.09 of the cumulative distribution shown in Figure 9.

It is important to note that, although the geometric size of both particle fractions (isometric and fibrous) of the MWCNT aerosol can be described by a lognormal distribution (monovariate or bivariate), the geometric size of their combined fractions in the total sample is not lognormally distributed. Figure 10 shows the number-based geometric size distribution of all the particles in a representative sample (combining Figure 4A and Figure 5 together). The two fractions of particles are clearly located in different regions of the width-length distribution and cannot be characterized by a unimodal size distribution. Although the overall MWCNT aerosol particles may fit to a bimodal, bivariate lognormal distribution and would be useful for dose calculation, this is beyond the scope of the present study and would not be discussed here. Nevertheless, the results do emphasize the importance of differentiating the overall MWCNT particles into different shape fractions (e.g. isometric and fibrous) and then characterizing each shape classification separately. Not only because the different shaped particles have different aerodynamic behavior in the air stream and distinct deposition patterns in the respiratory tract, but also because fiber-like shaped particles could have a much greater adverse effect on the lungs and other organs than the isometric particles. Information of this sort could be crucial in conducting detailed risk assessments. A similar approach may be useful when characterizing other engineered nanoparticles, since they tend to agglomerate during aerosol production and form particles with very different shapes and complex structures.

To make use of the data from the geometric size distributions and to check the consistency of different methods used in this study, the average dimensions obtained from the isometric and fibrous particles were used to estimate the count-based aerodynamic diameter for the overall particles. As an approximation, the diameter can be calculated based on average dimensions (100.3 nm/3.04 μm vs. 0.90 μm), effective densities (0.9 vs. 0.76 g/cm^3), and percent fraction (70 vs. 30%) of the fibrous and isometric particles. The densities can be obtained from Appendix A and Table 2, respectively, and the percent fractions from the ranges of 60–80 and 20–40%, respectively. The average dimensions of the count-based aerodynamic diameters were then calculated to be approximately 0.25 μm for fibrous particles [using Eq. (3, 4) shown in Cheng (1986) with the selection of parallel orientation], and to be approximately 0.77 μm for isometric particles [using Eq. (1)], and consequently,

an average of 0.41 μm for the overall particles. The closeness of this value (0.41 μm) to the count mode (0.42 μm) of the aerodynamic size distribution obtained from the impactor samples demonstrates the consistency of the results obtained from two different collection methods (impactor vs. filter) used in the study.

Aerodynamic size distribution

Aerodynamic size-segregated foil, filter, and grid samples were successfully collected using a MOUDI, while following explicit sample preparations and operating procedures. The total aerosol was characterized gravimetrically and examined microscopically using size selective foil and filter samples obtained with a MOUDI. Figure 6 shows a histogram of the mass-based aerodynamic size distribution of the aerosol derived from the foil samples. The distribution had a mean MMAD of 1.5 μm and a mean GSD of 1.67 with the assumption that the mass measurements can be described with a uni-modal lognormal distribution (the curve in Figure 6). It is important to point out that the contribution of particles less than 0.1 μm are ignored in this representation. Those particles may not be substantial in terms of their mass, but could be significant in terms of particle count.

The size-classified samples obtained with a MOUDI also showed that the aerodynamic size distribution had a mass peak on the 6^{th} stage (≈1.3 μm) based on gravimetric measurements and a number (count) peak on the 8^{th} stage (≈0.42 μm) based on microscopic observations. The reason that the mass-based mode is larger than the count (number)-based mode is that a few larger particles contribute disproportionately to the mass, whereas the smaller particles contribute more to the number. These data were used for qualitative comparisons with two near-real-time instruments (ELPI and SMPS).

Microscopic measurements of well-defined isometric and fibrous particles

The grid samples acquired from MOUDI filters samples were analyzed using a JEOL 1220 TEM. As described previously, MWCNT particles have complex shapes, including individual tube structures, clumped tube structures, and bundled rope structures. Only the well-defined isometric particles (with a compact structure and an aspect ratio less than or equal to 1.5) and fibrous particles (consisting of individual nanotubes) were included in this analysis because they were more easily classified.

Figure 7 shows, as expected, a trend of decreasing mean microscopic size for both isometric and fibrous particles in the impactor samples from stage 6 to 11. This clearly illustrates that the MOUDI was able to size classify MWCNT particles even though it could not effectively shape segregate the isometric particles from the fibrous particles. This qualitative observation is supported by the data listed in Table 2, which shows a decrease of the mean projected area diameter (d_{pa}) of isometric particles from 1.46 to 0.15 μm and a decrease in the mean length and width (L, W) of fibrous particles from (6.38 μm, 206 nm) to (1.38 μm, 52 nm) for increasing stage numbers. It should be noted, however, that the mean values of the measurements differed between stages, but there were significant variations with respect to the means as evidenced by the large values of the standard deviations given in the table. These results suggest that the sharp-cut characteristics normally displayed by a cascade impactor for aerosols of compact spheres may not apply for MWCNT's. This is another

indication that MWCNT aerosols contain a wide range of particle sizes and shapes, which makes aerodynamic classification challenging.

The large variations in particle size and shape on individual stages of the impactor were partially due to the relatively wide size classification range of each impactor stage. This could be reduced by using a size-classifying device with greater size discrimination capabilities, such as a differential mobility classifier. Although it was not the aim of this study, it would be interesting to size classify MWCNT's with such a classifier prior to introducing them into a MOUDI and then conducting a microscopic analysis with the size selected samples. This type of investigation may provide additional information on MWCNT particle characteristics due to the differences in the charging efficiency and electrical mobility between the fibrous and isometric particles.

Alternatively, since analyzing fiber-like and isometric particles was not sufficient to describe the entire population (only limited to well-defined particles) of MWCNT aerosol collected with the MOUDI, it may be useful to consider a third shape category during the microscopic measurements. This category may comprise the remaining irregularly-shaped particles (not the well-defined fiber-like and isometric particles) and, consequently, the entire size spectrum could be illustrated with a trimodal, bivariate distribution using the three shape classes. This approach will be considered in future investigations of the MWCNT's.

Effective particle density for isometric particles

Table 2 shows the means and standard deviations of the effective density of isometric particles calculated from the measured projected area diameters as determined by microscopy. Although the samples have a different mean value of d_{pa} on different stages, it would be expected that their relatively large standard deviations would result in a wide range of the calculated particle density, ρ_p. As predicted, calculated values of ρ_p varied between 0.50 and 0.88 g/cm^3 among stages. Besides the intrinsic complexity due to the diverse structures of MWCNT particles, this wide range of variation can be partly due to (1) the different compositions of the isometric particles measured and (2) the inadequacy of the aerodynamic diameter used in the calculation.

Detailed observations of the FE-SEM and TEM images (Figure 1F–1G and 7) showed that, even though the isometric particles under analysis were assumed to have a similar shape, they seemed to possess two different morphologies and textures: one was relatively compact and dense with a smooth surface like soot, while the other was more loosely packed with a clumped tube structure (Figure 1G). Particles with the former configuration tended to be smaller in projected area and larger in their effective density when compared to those with the latter morphologies. In addition, nodules containing metal catalysts (Figure 1G), although only contributing a trace amount (0.41% sodium and 0.32% iron) to the overall MWCNT mass (Porter et al., 2010), may represent a reasonable percentage of the number of the well-defined isometric particles. Consequently, the difference in the composition among the particles could contribute to the variation in the calculated density of those particles.

Another factor to be considered is that the aerodynamic diameter, which is defined as $d_{ae} = (d_{i-1} \times d_i)^{1/2}$, where d_i is the 50% cutoff diameter on i-th stage (Eq. (1)), may not be adequate to represent all the aerodynamic size-classified particle fractions. The size-classified particles on each impactor stage are normally considered to be lognormal in size for an aerosol whose aerodynamic size is represented by a lognormal distribution (Mercer, 1963; Hinds, 1986). The median diameter of the distribution on a given stage is equal to the geometric mean of the cutoff sizes of the current and upper stages. This is because particles collected are assumed to negotiate air streamlines on the upper stage, but not those on the stage under consideration. When the actual distribution of the particles collected on a stage is far from lognormal as in the case of the particle fractions on the edges of the overall distribution, this assumption is no longer valid. For example, the four particles collected on the 11th stage (N_p = 4; Table 2) were the only available isometric particles observed in the sample. They were the smallest particles in the classified isometric samples collected from stage 6 to stage 11. It appears that they are more closely related to a tiny fraction of particles which were primarily collected on the 10th stage, rather than those collected on the 11th stage. Even though they were collected on the 11th stage, it would be reasonable to characterize their aerodynamic behavior using the cutoff size of the 10th stage rather than using the geometric mean of the cutoff sizes of the 10th and 11th stages. This adjustment would only apply to samples with few particles to be analyzed, such as those in the uppermost and/or the lowest stage of the overall distribution. With this small modification, it is interesting to note that the mean density of the particles on the 11th stage increases from 0.50 to 0.71 g/cm^3, which is close to the mean values for the other stages. Keep in mind that this narrow range of the density values (0.71–0.88 g/cm^3) is only an estimation based on well-defined isometric particles in the MWCNT aerosol.

Dynamic shape factor for fibrous particles

The dynamic shape factor, κ, of individual nanotubes was determined by two different methods: (1) indirectly using Eq. (3) by substituting the aerodynamic diameter on a given stage based on the 50% cut-off diameters of compact spheres on the stages, or (2) directly using Eq. (4) by assuming the nanotube particle as a prolate spheroid moving in the air with a certain orientation. In Table 2, the dynamic shape factors determined using the first approach varied between stages, decreasing gradually from 2.50 for the particles on the 11th stage to less than unity for the particles on the 6th stage. The values of κ using the second approach were less variable, ranging from 1.94 to 2.71 between stages. Since a well-defined fibrous particle should have a mean κ value greater than unity, there appear to be discrepancies using the first approach. Even after the correction associated with the definition of aerodynamic diameter (Eq. (3)), the mean value of κ was still close to unity. This seems to indicate that the initial approach may not be applicable to the well-defined fibrous particles collected on stage 6. This discrepancy may be partly due to the fact that, when separating fibers using an impactor, the separation characteristics should consider both width and aspect ratio, rather than geometric or aerodynamic diameter alone (Asgharian et al., 1997) and thus Eq. (2) needs to be modified to result in an adequate κ. Table 2 shows the results from the 2nd approach are in agreement with those from the 1st approach, except for those of stages 6–8. Note that the values using the second approach were determined primarily based on parallel orientations of fiberlike particles except for those on the 11th

stage, in which random orientation was applied. Again, the values of the particle shape factor are only an estimation of individual nanotubes in the MWCNT aerosol. It would be difficult, if not impossible, to estimate the shape factors of all the MWCNT particles because of their complex structures.

Comparisons with ELPI and SMPS

Figure 8 shows representative number-based size distributions and concentrations of a total MWCNT aerosol taken from the exposure chamber with both ELPI and SMPS. Table 3 shows a detailed comparison between the results from the two near-real-time instruments and those from microscopic and gravimetric measurements derived from the filter and MOUDI samples. The agreements are reasonable for the count-based size distribution and number concentration, with the values of count mode and number concentration in the same order of magnitude: ELPI (0.43 μm and 3.4×10^4 particles/cm^3), SMPS (0.35 μm and 4.2×10^4 particles/cm^3) and MOUDI/filters (0.42 μm and 2.7×10^4 particles/cm^3). The closeness in the number concentration indicate that particle counting using electrical charge measurement (ELPI) or photometric sensing technique (SMPS) provided measurements of the same order of magnitude as those using microscopic measurements. The dissimilarities between methods may be attributed to the differences between the test MWCNT particles used in this study and the near-spherical compact particles used for manufacturer's calibrations. The similarity in the count mode between ELPI and MOUDI was expected, since both instruments classify particles according to their aerodynamic diameter. The differences between count measurements of the ELPI and MOUDI and those of SMPS most likely resulted from the SMPS classifying particles based on their electrical mobility equivalent diameter.

Differences between instruments based on mass are more noticeable. Compared to the gravimetric measurements from the MOUDI, that revealed a MMAD of 1.5 μm, a mass mode of 1.34 μm, and a mass concentration of 10 mg/m^3, the ELPI determined a larger MMAD (>2.0 μm), a larger mass mode (1.84 μm) and a higher mass concentration (≈20 mg/m^3) while SMPS measurements indicated a smaller mass mode (1.19 μm) and a lower mass concentration (3.2 mg/m^3). Since both near-real-time instruments use built-in algorithms to convert distributions by assuming particle geometry as compact spheres, the differences in data between instruments could be associated with the complex structures of the isometric and fibrous particles in the test MWCNT aerosol, as well as the two different equivalent diameters measured by the instruments. The reasons for the different responses between the two near-real-time instruments, i.e. higher values for ELPI but lower values for SMPS, are unknown and may be partially associated with the differences in the chargers (unipolar ion corona discharging vs. bipolar ion source) and how the charged particles were classified and detected.

Although the near-real-time instruments provide a reasonably close estimate of the number concentration of the particles in the total MWCNT aerosol, this information could be misleading when applying to risk assessment. As described previously, the number concentration based on total nanotubes would be a better metric than that based on total particles (or particle structures) when dealing with the biologically relevant dose. With this

in mind, use of the number concentration from a near-real-time instrument to interpret the biological effects resulting from inhalation exposure to engineered nanoparticles should be interpreted cautiously. This is especially important for the nanoparticles with highly agglomerated structures.

Estimation of human equivalent exposure

The information obtained from this study has been used to design inhalation exposure studies in rats (Stapleton et al., 2012). The deposited MWCNT doses in the alveolar region of laboratory animals were estimated to determine their relevancies to human occupational exposures. The deposited MWCNT dose was expressed as follows:

$$\text{Dose}=\text{Concentration}\times\text{minute}\quad\text{volume}\times\text{duration}\times\text{deposition}\quad\text{efficiency} \tag{8}$$

As an example of exposure to 5 mg/m^3 of MWCNT aerosol for 5 h, the resulting deposited dose in a rat is approximately 21 μg. This estimation was made by supposing that the rat minute volume was 214 mL/min (Brown et al., 2005) and particle deposition efficiency was 6–7% (MPPD, 2010; Raabe et al., 1988):

$$5\text{mg/m}^3\times(214\text{mL/min}\times10^{-6}\text{m}^3\text{mL})\times(5\text{h}\times60\text{min/h})\times0.065=21\mu\text{g}.$$

Assuming an alveolar epithelium surface area of 0.40 m^2 for a rat, the 21 μg MWCNT dose would result in 52.2 μg MWCNT/m^2 reaching the alveolar epithelium (Stone et al., 1992).

Similar calculations have been made to estimate the dose equivalents in standard workers, defined as 31 % sitting and 69% light exercise with a minute ventilation of 20 L (ICRP, 1994), for a standard 8-h work shift. The alveolar epithelium surface area of the worker was assumed to be 102.2 m^2 (Stone et al., 1992). If the MWCNT aerosol reached the initially proposed NIOSH recommended exposure limit (REL) of 7 μg/m^3 (NIOSH, 2010) and the mean deposition fraction was 11 % (ICRP, 1994; MPPD, 2010), the estimated human exposure per month (i.e. 8 h/day, 5 days/week, and 4.3 weeks/month) reaching the alveolar epithelium would be 0.97 μg MWCNT/m^2. Thus, 5 mg/m^3 MWCNT exposure of a rat for 5 h will be equivalent to human deposition for a male adult performing light work for 4.5 years, which is a reasonable human equivalent occupational exposure to MWCNT's. Note that the calculations were based on particle deposition only with no or little clearance from the lungs, which was a reasonable assumption for MWCNT's according to the results by Porter et al. (2012).

For the MWCNT exposure study in mice, the lung burden was experimentally determined one day after the exposure was concluded (Porter et al., 2012). For a 2-day exposure (i.e., 5 hours per day) at a mean concentration of 10 mg/m^3, the MWCNT lung burden was 6.6 μg. Assuming an alveolar epithelium surface area of 0.05 m^2 for a mouse, the 6.6 μg MWCNT dose would result in 132 μg MWCNT/m^2 reaching the alveolar epithelium (Stone et al., 1992). Using similar calculations described above, this MWCNT exposure scenario in mouse would approximate human deposition for a person performing light work for 11.3 years, while being exposed to a MWCNT aerosol of 7 μg/m^3. This estimate indicates that

mouse exposure to a MWCNT concentration of 10 mg/m^3 for 10 h would provide a reasonable human equivalent occupational exposure to MWCNT. Similar estimate can be conducted using the number of nanotubes instead of the mass concentration by relating 10 mg/m^3 to 4.9 × 10^5 nanotubes/cm^3 [i.e. 1 μg ≈ 4.9 × l0^7 nanotubes].

There is concern on the use of 10 mg/m^3 in the present study and subsequent animal exposures because this concentration is high relative to that of 440 μg/m^3 occurring in a workplace (Han et al., 2008), In fact, besides 10 mg/m^3, we have also conducted inhalation studies at an exposure level of 5–0.5 mg/m^3. For the low concentrations, the same methods of generation and characterization described in the present study were used. Even though the degree of agglomeration could vary with the concentration and consequently change the particle size distribution, our results indicate that the distribution of particle structures are similar, with MMADs of 1.4 and 1.6 μm, respectively, for 0.5 and 5 mg/m^3 compared to a MMAD of 1.5 μm for 10 mg/m^3 reported previously. Filter samples at low concentrations were also collected and will be analyzed later using an electron microscope. The results will be compared with that of 10 mg/m^3.

Summary

A computer-controlled MWCNT aerosol generation and inhalation exposure system (McKinney et al., 2009) was used in this study. The system is capable of continuously generating consistent concentrations (3–12 mg/m^3) of a MWCNT aerosol for extended periods of time (5 h/day, 5 days/week, for up to 4 weeks). The daily relative standard variation in aerosol concentration was less than 2% and the day-to-day variation was less than 5%. FE-SEM/TEM micrographs of filter samples collected from the exposure test chamber showed that particle morphologies within the generated aerosol were complex and diverse in shape and structure. The size and shape of the MWCNT's were comparable with those previously shown to be present in occupational environments. Due to health concerns resulting from their fiber-like morphology, special guidelines were established for sampling the MWCNT aerosol on filters for microscopic counting and sizing (surface density of 0.008 – 0.10 particles/μm^2). In addition to analyzing filter samples, size-classified samples were collected on various media using a cascade impactor, which was operated under special conditions developed for characterizing the particles. Results indicated that an aerosol of 10 mg/m^3 contained a number concentration of 2.7 × 10^4 particles/cm^3. There was a mean value of 18 nanotubes per particle, indicating a high degree of agglomeration, which resulted in approximately 4.9 × 10^5 nanotubes/cm^3. Due to the complexity of the particle morphology, the particles were separated in two categories, which included isometric and fibrous particles. The isometric particle size followed a lognormal distribution with a CMD_G of 0.90 μm and a GSD of 2.08, while the length and width of the fibrous particles followed a bivariate lognormal distribution with a CML of 3.04 μm (GSD_L = 2.23) and a CMW of 100.3 nm (GSD_W = 1.73). By combining the two geometric size distributions from the microscopic analysis of isometric and fibrous particles, the average aerodynamic diameter of the overall particle distribution can be approximated to be 0.41 μm by substituting the average dimension, effective density, and percent fraction of each shape category. Results from the MOUDI impactor indicate that the overall particle size distribution of the MWCNT aerosol had a MMAD of 1.5 μm with a GSD of 1.67, or a mass mode of 1.3 μm and a count

mode of 0.42 μm. The closeness of this count mode (0.42 μm) to that (0.41 μm) estimated from the two geometric size distributions verifies the consistency of the results obtained from two different collection methods (impactor vs. filter) used in the study. Although measurements of particles collected on different impactor stages vary considerably, the mean effective density of the well-defined isometric particles has a narrow range of between 0.71 and 0.88 g/cm^3 and the mean shape factor of the well-defined individual nanotubes has a range between 1.94 and 2.71. Results of number-based size distribution and concentrations measured with two near-real-time instruments (ELPI and SMPS) were in reasonable agreement with microscopic measurements. Information obtained from this study has been used to design animal inhalation exposure studies to selected doses that would be relevant to those experienced by humans during potential occupational exposure scenarios. The intention of this study was to develop protocols that could be used for aerosol sampling and characterizing MWCNT particles, as well as other engineered nanoparticles.

Supplementary Material

Refer to Web version on PubMed Central for supplementary material.

Acknowledgements

The authors would like to thank Amy Cumpston and Donny Leonard (NIOSH) for helping with the experiments and Mr. Owen Price and Dr. Bahman Asgharian for useful discussion on the MPPD model and the data interpretation.

Appendix A: Estimation of the number concentration of a MWCNT aerosol based on its mass concentration

The number concentration of a MWCNT aerosol can be calculated from its mass concentration if the particle size distribution follows a lognormal distribution. Then the average size and average mass of the particles can be estimated with this information (Hatch & Choate, 1929; Chen et al., 1990). The relationship is more complicated for fiber-like particles, because additional information is needed concerning their width and length. The following calculations use available information, describing the length and width of individual carbon nanotubes, to estimate their number concentration based on their mass concentration.

A description of an average single MWCNT was obtained from the lattice image of the graphene structure shown in the high resolution TEM micrograph [Figure 1 in Porter et al. (2010)]. The width of the inner hollow core (W_C) was 5.385 nm, the thickness of each graphene sheet (W_T) was 0.166 nm, and the distance between two graphene layers (W_D) was 0.222 nm. Even though these measurements were based on photographic images, they could be biased by the size limitation of their resolution. The measured values, however, seem to be in reasonable agreement with the information provided by the manufacturer. The data, that were made available, gave an average inner core dimension of 5.0 nm and the average distance from the center of one sheet to the center of the next sheet was 0.3385 nm (Kim et al., 2005). These measurements were used to determine the number of graphene sheets and the volume of a single MWCNT with a known length and width. As an example, MWCNT's

having widths of 21, 49, and 66 nm consisted of 21, 57, and 79 graphene sheets or layers, respectively. Figure 11 shows the relationship of the number of graphene layers versus the fiber density (ρ_p) of a single nanotube (with voids) observed in the study, as a function of the width of the nanotube. That relationship was calculated based on physical measurements of W_C, W_T, and W_D from the electron micrographic images. The number of graphene sheets increases linearly with tube width (solid line), whereas the fiber density per nanotube (dashed line) increases asymptotically with tube width and quickly reaches a constant value of 0.9 g/cm^3 for widths greater than 40 nm. The two curves in Figure 11 have the same shape for various combinations of W_C, W_T, and W_D with the exception that the constant asymptotic value of particle density is a function of W_C, W_T, and W_D.

Results from Porter et al. (2010) indicate that individual MWCNT's have a count mean width of 49 nm (SD = 13.4) and a count median length of 3.86 μm (GSD = 1.94). Assuming that a nanotube with these dimensions represents a fiber with an average mass, the average volume per nanotube (without voids) would be 6.0×10^6 nm^3 (Cheng, 1986). Note that this estimate is based on assuming a bivariate lognormal distribution for the width and length of fiber-like particles having a correlation value of 0.5.

The manufacturer indicated that the average MWCNT density (specific gravity) measured with a pycnometer was 2.1 g/cm^3. Because the nitrogen molecules used in the device were able to penetrate through the voids between the graphene sheets, this value represents the material density (without voids) of the nanotube. Using this value of specific gravity, the average mass per nanotube (excluding voids) is 1.23×10^{-1} mg.

Making the assumptions described above, a mass concentration of a 10 mg/m^3 aerosol of total MWCNT's would correspond to 8.0×10^5 nanotubes/cm^3. This value represents the total number of nanotubes in the aerosol, not the total number of particles. Since multiple nanotubes form agglomerate, which are counted as one particle ("CNT structure"), the number concentration of particles depends on the average number of nanotubes per particle. As an example, assume that each particle contains an average number of 10 nanotubes, then the aerosol concentration would contain about 8.0×10^4 particles/cm^3. Bear in mind that the accuracy of the results obtained from these calculations is based on the single MWCNT characteristics described by Porter et al. (2010). A more accurate value of particle concentration using the average value of 18 nanotubes per particle (described in the text) would result a concentration of 4.4×10^4 particles/cm^3.

Appendix B: Development of a sampling/operation protocol for microscopic observations of MWCNT particles

The NIOSH standard 7402 (NIOSH, 1994a) asbestos fiber measurement method using membrane filters and microscopic analysis was initially adopted as a guideline for quantitatively describing MWCNT aerosols. Initially, polycarbonate filters of 2.5 μm pore size (Whatman, Clinton, PA) were used for collecting MWCNT samples from the chamber at a flow rate of 1 L/min. Polycarbonate filters were used because of their smooth surface, which was advantageous for microscopic observation of particles. After sampling, the loaded filters were cut into four pieces and mounted onto aluminum stubs with double-stick

carbon tape, and coated with gold/palladium using a SPI sputter coater (SPI-Module, Structure Probe Inc., West Chester, PA). The samples were then analyzed using a field emission scanning electron microscope (FE-SEM; Hitachi, S-4800, Tokyo, Japan). A FE-SEM, rather than a transmission electron microscope (TEM), was used to observe the samples. This FE-SEM is capable of providing information concerning the 3-dimensional morphology of the particle, as well as estimating the number of nanotubes incorporated in each particle. Figure 1C–1D show the images of aerosol particles collected on filters of 2.5 μm pore size. The sample appears to contain particles of many different shape configurations including single smooth nanotubes with various aspect ratios (*L/W*, *L* = length and *W* = width or diameter), bundled nanotubes, nanotube nodules (fiber-like particles having nano-sized nodules attached), and isometric-shape or fiber-like agglomerates having nanotubes and/or compact particles attached. While the “individual nanotubes” are easy to identify as fiber-like particles that contain mainly elemental carbon, the agglomerates (“CNT structures”) could consist of nanotubes, nodules, and/or compact particles with heterogeneous compositions. Figure 1H shows the particles are primarily composed of elemental carbon using energy dispersive X-ray analysis (SEM-EDX; Princeton Gamma-Tech, Rocky Hill, NJ). Figure 1G illustrates that, at a magnification of ×40K, the nano-sized nodules (right in the figure) attached to the nanotubes are likely to be residual metal catalyst seeds from the growth process, and the micron-sized compact particles (left in the figure) with a smooth surface are believed to be soot resulting from the condensation of carbon-containing vapor.

Although the sample in Figure 1C contains a good representation of particles with diverse morphologies, the images of the particles distributed on the filter surface clearly illustrate that the sample was overloaded during collection. This condition makes it difficult for identifying individual particles and determining their size. This sample also indicates that the use of filters with a 2.5 μm pore size may allow ultrafine nanotube particles to deposit inside the pore (Figure 1D) or even penetrate through the pores and cause underestimate when counting the nano-sized fraction of the MWCNT aerosol. Due to these shortcomings, modifications to the NIOSH standard 7402 are needed to provide adequate filter samples with high collection efficiency and optimal distribution for microscopic observations of MWCNT’s. The important issues related to filter sampling and microscopic operation are listed below:

1. Selection of filters: In order to improve the sampling techniques for particle quantification, filters with a 0.1 μm pore size (Whatman) were selected for this study. The filters were mounted in a closed-face filter holder with a 5-cm electrically conductive plastic extension cowl. This filter assembly was used for collecting MWCNT samples for particle counting, sizing, and morphological analysis with the FE-SEM (Hitachi). The small pore size polycarbonate filter has a collection efficiency of greater than 99% for ultra-fine aerosol particles (Liu et al., 1983). As a tradeoff for the high pressure drop across the filter, however, the sampling flow rate was reduced to 0.4 L/min.
2. Microscopic observation: The FE-SEM images in Figure 1C–1G indicate that MWCNT aerosol contains a mixture of individual nanotubes and particles with

agglomerated structures which represent a broad size spectrum between 40 nm and 10 μm. This required an electron microscope operated under an extensive range of different magnifications (see Figure 1E–1G). The lower range was used to determine the micrometer-sized length of nanotubes and agglomerates under a lower magnification (e.g. ×2K and ×5K), while the upper range was used to determine the nanometer-sized width of individual nanotubes under a higher magnification (e.g. ×40K).

3. Optimal surface density: To minimize the sample overloading on filter during collection like the one shown in Figure 1C, an ideal range of surface density should be determined. Unlike the deposit range of 100–1300 fibers/mm^2 as described in the NIOSH method for counting asbestos, the MWCNT aerosol contains particles of a smaller size and requires a denser deposit on filter for proper microscopic observations. At a flow rate of 0.4 L/min, different time intervals and sampling volumes were chosen to produce an optimal surface density on filter for microscopic observations. After several trials, a range of 0.008–0.10 particles/μm^2 was selected based on the ease and ability of counting FE-SEM images of particles on the filter. The surface density was determined by microscopically counting the number of particles and particle structures across an effective sample area on the filter surface.

4. Sampling time interval: The ideal range of a sampling time was estimated using the number concentration of MWCNT particles in the sampling volume. Although the number concentration associated with the mass concentration targeted at 10 mg/m^3 was not immediately available, it could be approximated by converting particle mass to particle number using previously published information (Porter et al., 2010) combined with assumptions that have been used previously for fibrous particles (Cheng, 1986). Details of the method of estimating particle number from mass measurements are described in Appendix A. Results of those calculations show that the estimate of the number concentration was 8.0×10^4 particles/cm^3 for a mass concentration of 10 mg/m^3. Consequently, a series of sampling time intervals between 5 s and 2 min were selected for the initial trials. It should be noted that this estimation was based on an assumption that there was an average of 10 nanotubes per particle.

References

Asgharian B, Zhang L, Fang CP. Theoretical calculations of the collection efficiency of spherical particles and fibers in an impactor. J Aerosol Sci. 1997; 28:277–287.

ASTM B922-10. Standard Test Method for Metal Powder Specific Surface Area by Physical Adsorption. West Conshohocken, PA: ASTM International; 2010a. 2010 www.astm.org

ASTM B923-10. Standard Test Method for Metal Powder Skeletal Density by Helium or Nitrogen Pycnometry. West Conshohocken, PA: ASTM International; 2010b. 2010 www.astm.org

Baron, PA.; Sorensen, CM.; Brockmann, JE. Nonspherical particle measurements: shape factors, fractals, and fibers. Chapter 23. In: Baron, PA.; Willeke, K., editors. Aerosol measurement: Principles, Techniques and Applications. New York: John Wiley and Sons, Inc; 2001. p. 705-749.

Baron PA, Deye GJ, Chen BT, Schwegler-Berry D, Shvedova AA, Castranova V. Aerosolization of single-walled carbon nanotubes for an inhalation study. InhalToxicol. 2008; 8:751–760.

Brown JS, Wilson WE, Grant LD. Dosimetric comparisons of particle deposition and retention in rats and humans. Inhal Toxicol. 2005; 17:355–385. [PubMed: 16020034]

Chen BT, Namenyi J, Yeh HC, Mauderly JL, Cuddihy RG. Physical characterization of cigarette smoke aerosol in a Walton smoke machine. Aerosol Sci Technol. 1990; 12:364–375.

Cheng YS. Bivariate lognormal distribution for characterizing asbestos fiber aerosols. Aerosol Sci Technol. 1986; 5:359–368.

Donaldson K, Aitken R, Tran L, Stone V, Duffin R, Forrest G, Alexander A. Carbon nanotubes: a review of their properties in relation to pulmonary toxicology and workplace safety. Toxicol Sci. 2006; 92:5–22. [PubMed: 16484287]

Endo M, Strano MS, Ajayan PM. Potential applications of carbon nanotubes. Carbon Nanotubes. 2008; 111:13–61.

Gallily I, Schiby D, Cohen AH, Holländer W, Schless D, Stöber W. On the inertial separation of nonspherical aerosol particles from laminar flows. I. The cylindrical case. Aerosol Sci Technol. 1986; 5:267–286.

Han JH, Lee EJ, Lee JH, So KP, Lee YH, Bae GN, Lee SB, Ji JH, Cho MH, Yu IJ. Monitoring multiwalled carbon nanotube exposure in carbon nanotube research facility. Inhal Toxicol. 2008; 20:741–749. [PubMed: 18569096]

Hatch T, Choate SP. Statistical description of the size properties of non-uniform particulate substances. J Franklin Inst. 1929; 207:369.

Hinds, WC. Data analysis. Chapter 3. In: Lodge, JP.; Chan, TL., editors. Cascade Impactors: Sampling and Data Analysis. Akron, OH: American Industrial Hygiene Association; 1986. p. 45-78.

Hou PX, Xu ST, Ying Z, Yang QH, Liu C, Cheng HM. Hydrogen adsorption/desorption behavior of multi-walled carbon nanotubes with different diameters. Carbon. 2003; 41:2471–2476.

ICRP. Human respiratory tract model for radiological protection: A report of a task group of the International Commission on Radiological Protection (ICRP). Vol. 24. Oxford: ICRP publication 66. Annals ICRP; 1994. p. 1-482.

Iijima S. Helical microtubules of graphitic carbon. Nature. 1991; 354:56–58.

Kim YA, Hayashi T, Endo M, Kaburagi Y, Tsukada T, Shan J, Osato K, Tsuruoka S. Synthesis and structural characterization of thin multi-walled carbon nanotubes with a partially facetted cross section by a floating reactant method. Carbon. 2005; 43:2243–2250.

Li JG, Li WX, Xu JY, Cai XQ, Liu RL, Li YJ, Zhao QF, Li QN. Comparative study of pathological lesions induced by multiwalled carbon nanotubes in lungs of mice by intratracheal instillation and inhalation. Environ Toxicol. 2007; 22:415–421. [PubMed: 17607736]

Liu, BYH.; Pui, DYH.; Rubow, KL. Characteristics of air sampling filter media. Chapter 70. In: Liu, BYH.; Marple, VA., editors. Aerosols in the Mining and Industrial Work Environments. Ann Arbor, MI: Ann Arbor Science; 1983. p. 989-1038.

Ma-Hock L, Treuman n S, Strauss V, Brill S, Luizi F, Mertler M, Wiench K, Gamer AO, van Ravenzwaay B, Landsiedel R. Inhalation toxicity of multiwall carbon nanotubes in rats exposed for 3 months. Toxicol Sci. 2009; 112:468–481. [PubMed: 19584127]

McKinney W, Chen B, Frazer D. Computer controlled multiwalled carbon nanotube inhalation exposure system. Inhal Toxicol. 2009; 21:1053–1061. [PubMed: 19555230]

Mercer RR, Scabilloni J, Wang L, Kisin E, Murray AR, Schwegler-Berry D, Shvedova AA, Castranova V. Alteration of deposition pattern and pulmonary response as a result of improved dispersion of aspirated single-walled carbon nanotubes in a mouse model. Am J Physiol Lung Cell Mol Physiol. 2008; 294:L87–L97. [PubMed: 18024722]

Mercer TT. On the calibration of cascade impactors. Ann Occup Hyg. 1963; 6:1–14. [PubMed: 13934934]

Mitchell LA, Gao J, Wal RV, Gigliotti A, Burchiel SW, McDonald JD. Pulmonary and systemic immune response to inhaled multiwalled carbon nanotubes. Toxicol Sci. 2007; 100:203–214. [PubMed: 17660506]

Motta M, Li YL, Kinloch I, Windle A. Mechanical properties of continuously spun fibers of carbon nanotubes. Nano Lett. 2005; 5:1529–1533. [PubMed: 16089483]

MPPD. Multiple-Path Particle Dosimetry Model, Version 2.11. Albuquerque, NM: Applied Research Associates, Inc; 2010. http://www.ara.com/products/mppd.htm

National Institute for Occupational Safety and Health (NIOSH). NIOSH Manual of Analytical Methods. 4th Ed. Cincinnati: National Institute for Occupational Safety and Health; 1994a. Asbestos by TEM Method 7402.

National Institute for Occupational Safety and Health (NIOSH). NIOSH Manual of Analytical Methods. 4th Ed. Cincinnati: National Institute for Occupational Safety and Health; 1994b. Asbestos and Other Fibers by PCM Method 7400.

National Institute for Occupational Safety and Health (NIOSH). Current Intelligence Bulletin: Occupational Exposure to Carbon Nanotubes and Nanofibers. DHHS (NIOSH) Publication. 2010. No. 2010-draft, December, 2010. http://www.cdc.gov/niosh/docket/review/docket161A/pdfs/carbonNanotubeCIB_PublicReviewOfDraft.pdf

Oberdörster G, Maynard A, Donaldson K, Castranova V, Fitzpatrick J, Ausman K, Carter J, Karn B, Kreyling W, Lai D, Olin S, Monteiro-Riviere N, Warheit D, Yang H. Research Foundation/Risk Science Institute Nanomaterial Toxicity Screening Working Group. Principles for characterizing the potential human health effects from exposure to nanomaterials: elements of a screening strategy. Part Fibre Toxicol. 2005; 2:8. [PubMed: 16209704]

O'Shaughnessy PT, Raabe OG. A Comparison of cascade impactor data reduction methods. Aerosol Sci Technol. 2003; 37:187–200.

Pauluhn J. Subchronic 13-week inhalation exposure of rats to multiwalled carbon nanotubes: toxic effects are determined by density of agglomerate structures, not fibrillar structures. Toxicol Sci. 2010; 113:226–242. [PubMed: 19822600]

Porter DW, Hubbs AF, Chen BT, McKinney W, Mercer R, Wolfarth M, Battelli LA, Wu N, Sriram K, Leonard SS, Andrew ME, Schwegler-Berry DE, Willard PA, Tsuruoka S, Endo M, Tsukada T, Munekane F, Frazer DG, Castranova V. Acute pulmonary dose-responses to inhaled multi-walled carbon nanotubes. Nanotoxicology. 2012 [Epub ahead of print].

Porter DW, Hubbs AF, Mercer RR, Wu NQ, Wolfarth MG, Sriram K, Leonard S, Battelli L, Schwegler-Berry D, Friend S, Andrew M, Chen BT, Tsuruoka S, Endo M, Castranova V. Mouse pulmonary dose- and time course-responses induced by exposure to multi-walled carbon nanotubes. Toxicology. 2010; 269:136–147. [PubMed: 19857541]

Raabe OG, Al-Bayati MA, Teague SV, Rasolt A. Regional deposition of inhaled monodisderse coarse and fine aerosol particles in small laboratory animals. Ann Occup Hyg. 1988; 32:53–63.

Ryman-Rasmussen JP, Tewksbury EW, Moss OR, Cesta MF, Wong BA, Bonner JC. Inhaled multiwalled carbon nanotubes potentiate airway fibrosis in murine allergic asthma. Am J Respir Cell Mol Biol. 2009; 40:349–358. [PubMed: 18787175]

Sager TM, Porter DW, Robinson VA, Lindsley WG, Schwegler-Berry DE, Castranova V. Improved method to disperse nanoparticles for in vitro and in vivo investigation of toxicity. Nanotoxicology. 2007; 1:118–129.

Schneider T, Holst E, Skotte J. Size distributions of airborne fibres generated from man-made mineral fibre products. Ann Occup Hyg. 1983; 27:157–171. [PubMed: 6614727]

Stapleton PA, Minarchick V, Cumpston AM, McKinney W, Chen BT, Sager T, Frazer D, Andrew M, Castranova V, Nurkiewicz TR. Impairment of coronary arteriolar endothelium-dependent dilation after multi-walled carbon nanotube inhalation: a time-course study. Int J Mol Sci (Submitted). 2012

Stöber, W. Dynamic shape factors of nonspherical aerosol particles. Chapter 14. In: Mercer, TT.; Morrow, PE.; Stöber, W., editors. Assessment of Airborne Particles: Fundamentals, Applications, and Applications to Inhalation Toxicity. Springfield IL: Charles C. Tomas; 1972. p. 249-289.

Stone KC, Mercer RR, Gehr P, Stockstill B, Crapo JD. Allometric relationships of cell numbers and size in the mammalian lung. Am J Respir Cell Mol Biol. 1992; 6:235–243. [PubMed: 1540387]

Thess A, Lee R, Nikolaev P, Dai H, Petit P, Robert J, Xu C, Lee YH, Kim SG, Rinzler AG, Colbert DT, Scuseria GE, Tomanek D, Fischer JE, Smalley RE. Crystalline Ropes of Metallic Carbon Nanotubes. Science. 1996; 273:483–487. [PubMed: 8662534]

Wang L, Castranova V, Mishra A, Chen B, Mercer RR, Schwegler-Berry D, Rojanasakul Y. Dispersion of single-walled carbon nanotubes by a natural lung surfactant for pulmonary *in vitro* and *in vivo* toxicity studies. Part Fibre Toxicol. 2010; 7:31. [PubMed: 20958985]

Warheit DB. How meaningful are the results of nanotoxicity studies in the absence of adequate material characterization? Toxicol Sci. 2008; 101:183–185. [PubMed: 18300382]

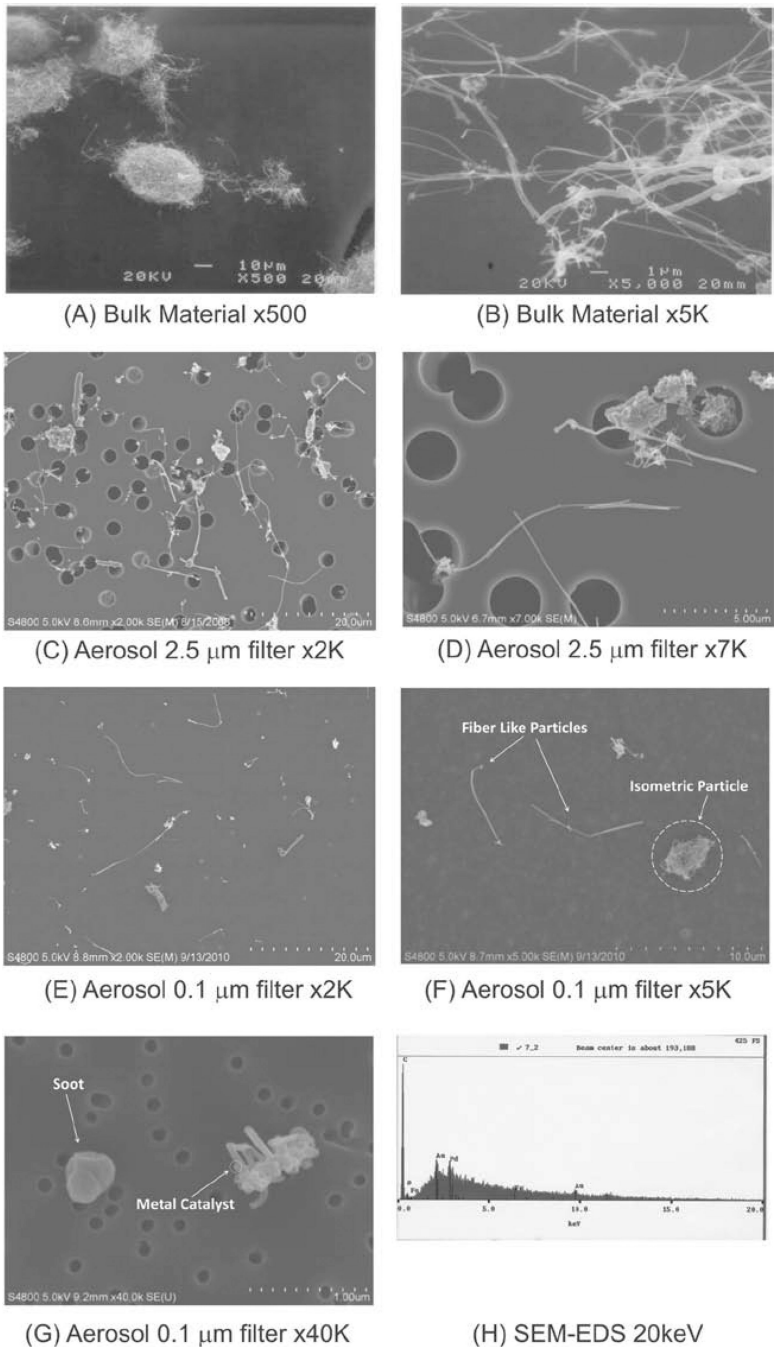

Figure 1.

Scanning Electron photomicrographs of MWCNT's: (A) bird-nest configuration in bulk material (non-dispersed), bar length = 10 μm; (B) bundled-together formation in bulk material (non-dispersed), bar length = 1 μm; (C–G) representative samples of aerosol particles generated from the acoustic disperser, collected using two different pore size filters (2.5 vs. 0.1 μm) with various magnifications (×2k–×40k), the full range of the tick marks are 20, 10, 5, and 1 μm, respectively; (H) SEM-EDX analysis indicates that the particles contain primarily carbon (gold and palladium are elements in the coating material).

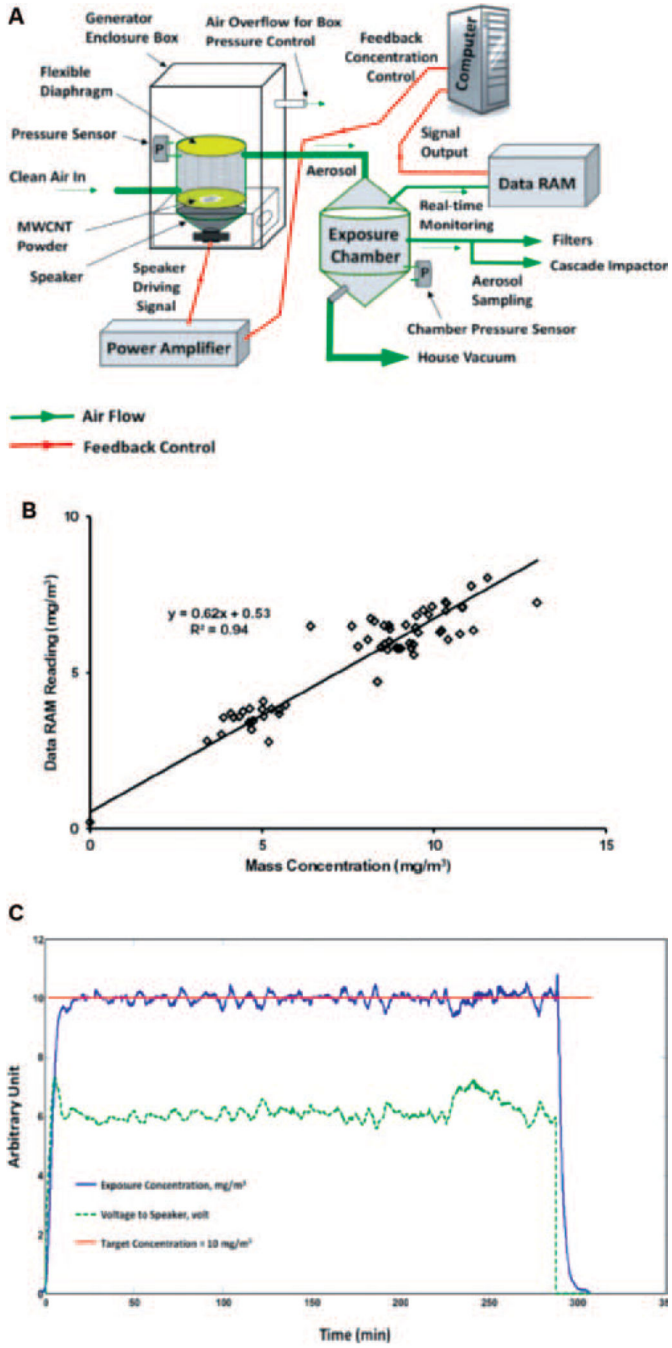

Figure 2.

(A) Schematic of a NIOSH MWCNT exposure system including an acoustical generator, exposure (sampling) chamber, and a feedback system; (B) Relationship between the readings from Data RAM and mass concentrations gravimetrically measured from PTFE filters; and (C) A real-time profile of speaker driving voltage and MWCNT concentration in the chamber with a target concentration of 10 mg/m^3. The actual concentration (mean ± standard deviation) was 10.02 ± 0.19 mg/m^3 with a daily range of 9.4–10.5 mg/m^3. Also shown is the output voltage to the speaker of the acoustic generator. The inverse relationship

between the voltage profile and the concentration profile indicates that the feedback system worked as expected.

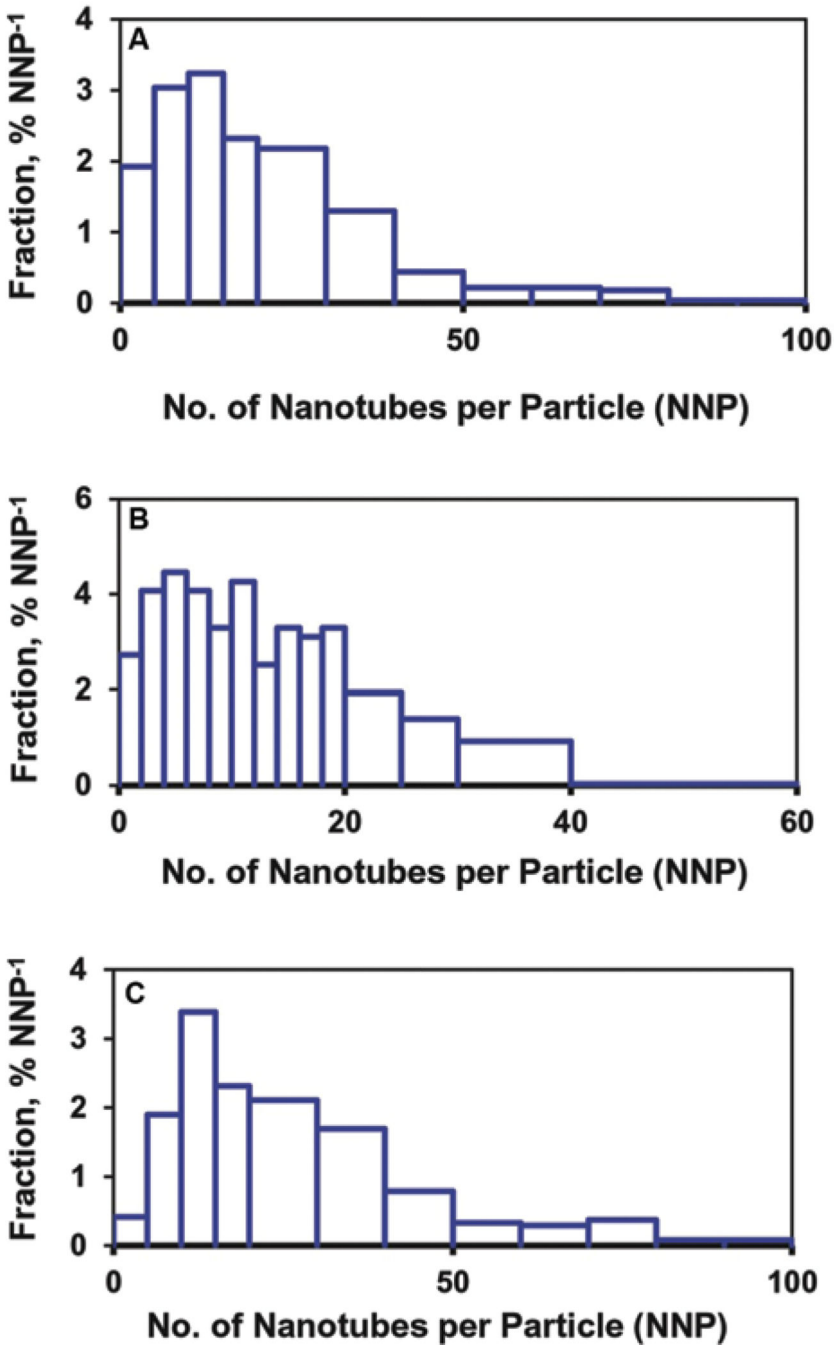

Figure 3.

Graphical representation of the distribution of number of nanotubes per particle (NNP) in a MWCNT sample: (A) total particles, (B) fibrous particles and (C) isometric particles. The fraction per unit x-axis interval (% NNP^{-1}) is plotted as the height of the histogram. Distribution of total particles (A) follows lognormal statistics with a count median NNP of 16 and a geometric standard deviation of 2.1.

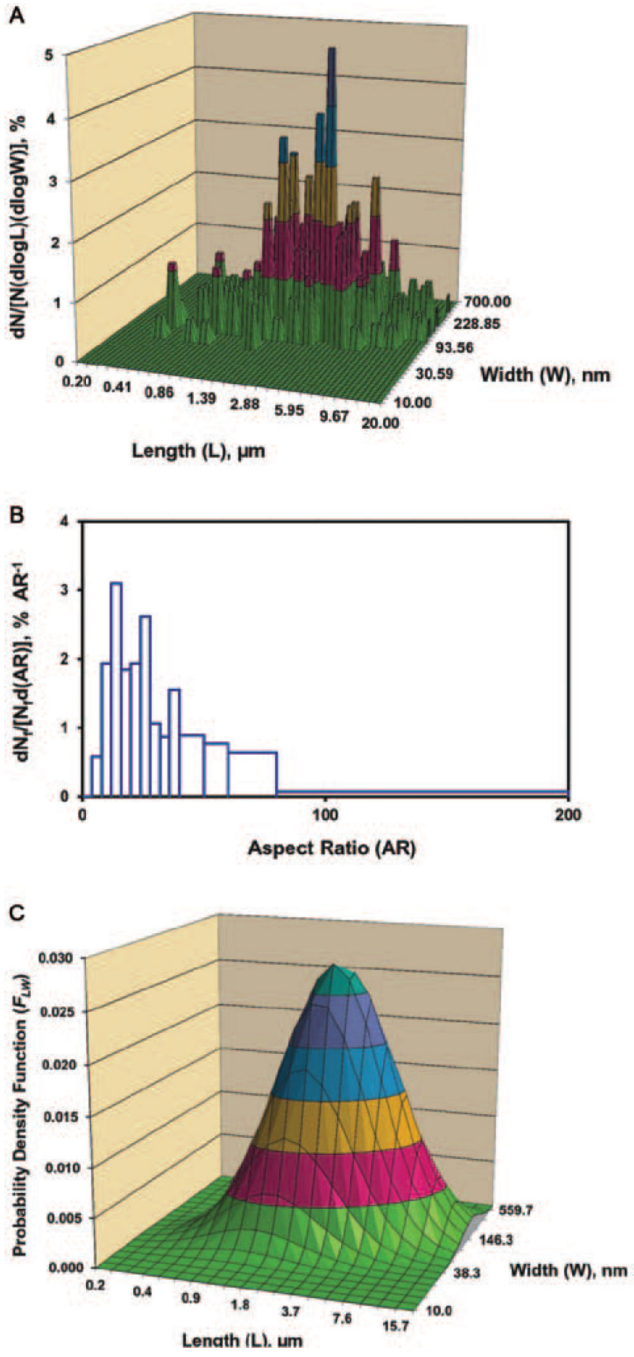

Figure 4.

The distribution of fiber-like particles in a representative MWCNT aerosol sample collected from the animal exposure chamber. (A) Number-based size distribution. The curve shows the percent number concentration per unit length and unit width interval (N = number concentration, L = fiber length, and W = fiber width). Different colors represent different z-values (ranging from 0 to 5 in an increment of l).(B) Distribution of the aspect ratio, L/W (N_f = number of particles). (C) Probability density function (F_{LW}) of the bivariate lognormal distribution for fiber-like particles in the MWCNT aerosol using the following parameters:

count median width (CMW) = 100.3nm (GSD_W = 1.73), count median length (CML) = 3.04 μm (GSD_L = 2.23), and correlation (τ) = 0.47. Different colors represent different F_{LW} values (ranging from 0 to 0.03 in an increment of 0.005).

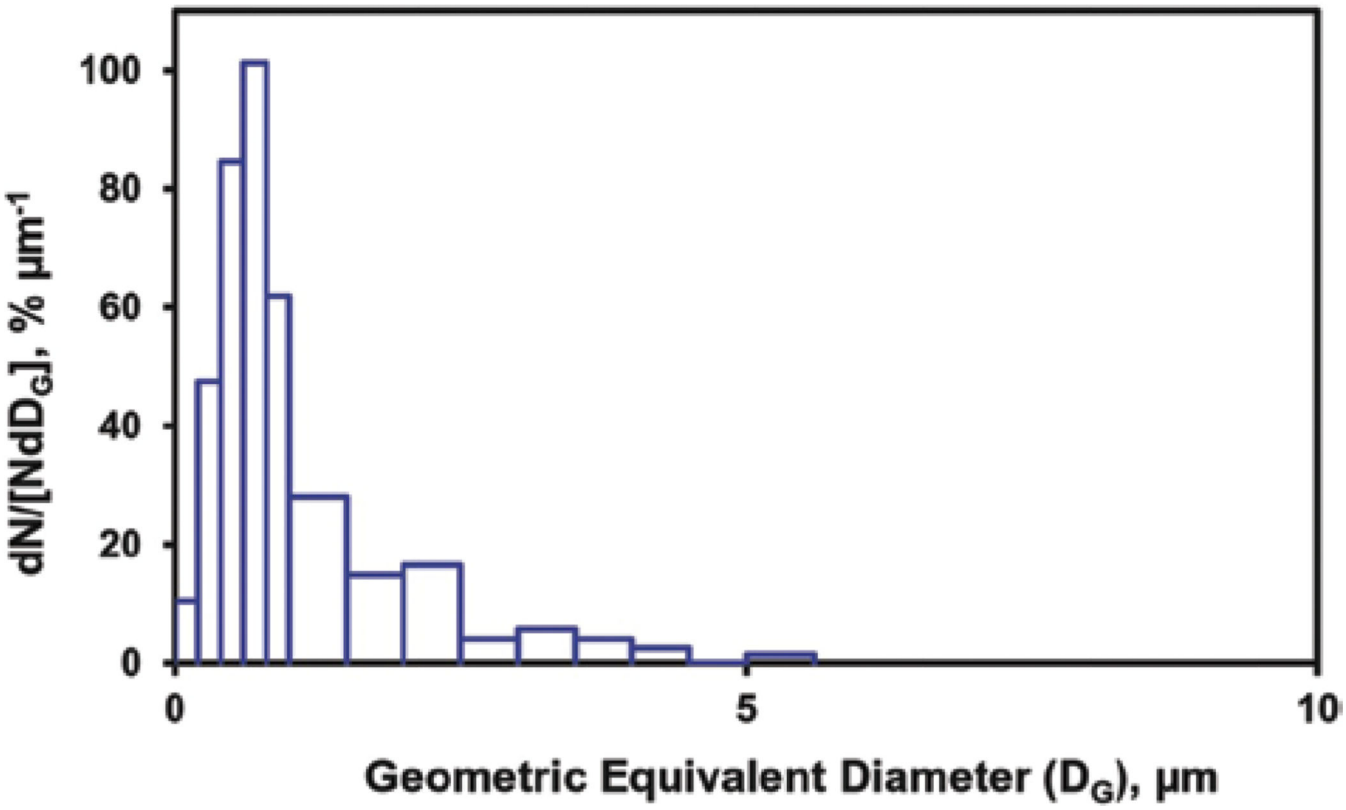

Figure 5.

Number-based size distribution of the isometric particles in the MWCNT aerosol collected from the animal exposure chamber. The histogram shows the percent number concentration per unit size interval (N = number concentration, D_G = geometric equivalent diameter). The distribution can be lognormally expressed with a count median diameter (CMD_G) of 0.90 μm and a geometric standard deviation (GSD) of 2.08.

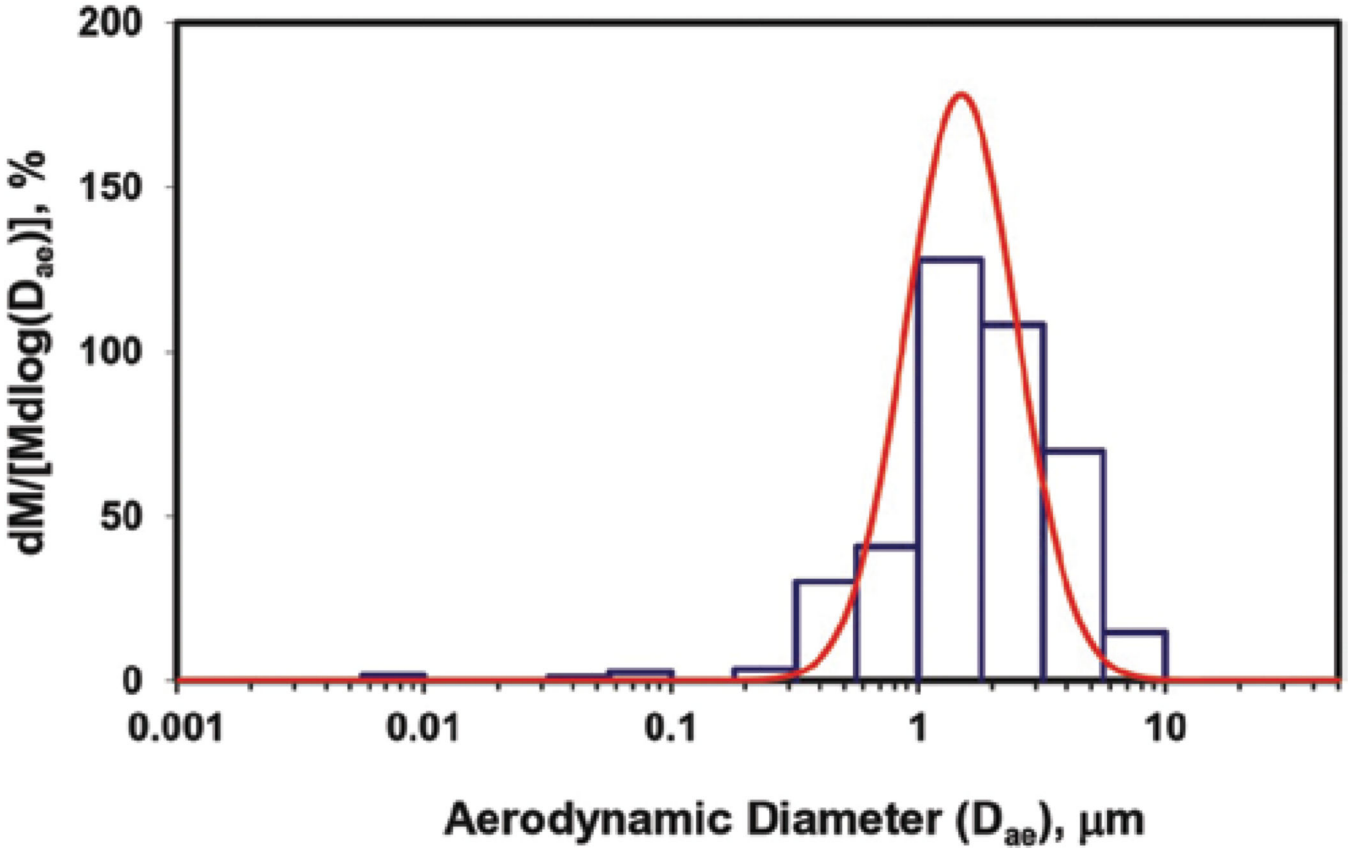

Figure 6.

A typical particle size distribution of the MWCNT aerosol in the sampling chamber. The histogram shows the percent mass concentration per unit size interval (*M* = mass concentration, D_{ae} = aerodynamic diameter) obtained from MOUDI and the curve indicates the expression of the primary size mode under the assumption of a lognormal distribution, which results in a MMAD of 1.50 μm and a GSD of 1.67. A mass mode of 1.34 μm and a count mode of 0.42 μm were qualitatively determined from the distribution.

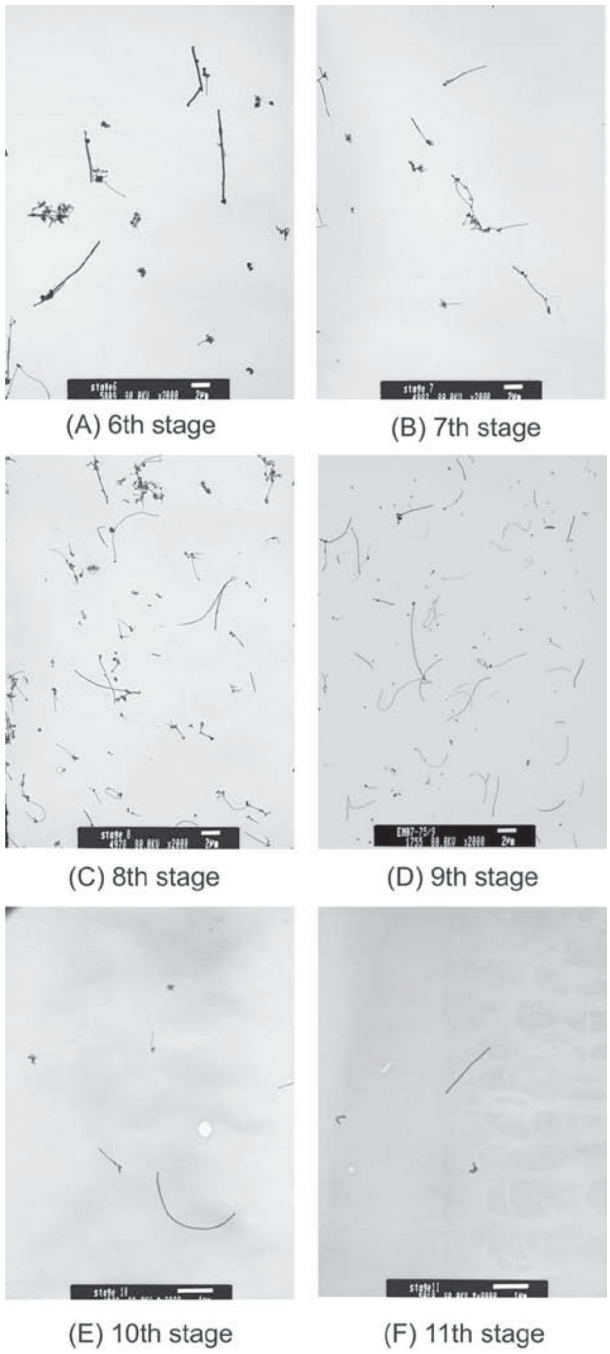

Figure 7.

TEM photomicrographs of particles collected on the grids of MOUDI stages 6–11 (A–F). The scale bars are 2 μm on A–D and 1 μm on E–F. The 50% cutoff diameters, d_{50}, on stages 6–11 are 1.0, 0.56, 0.32, 0.18, 0.10, 0.056 μm, respectively.

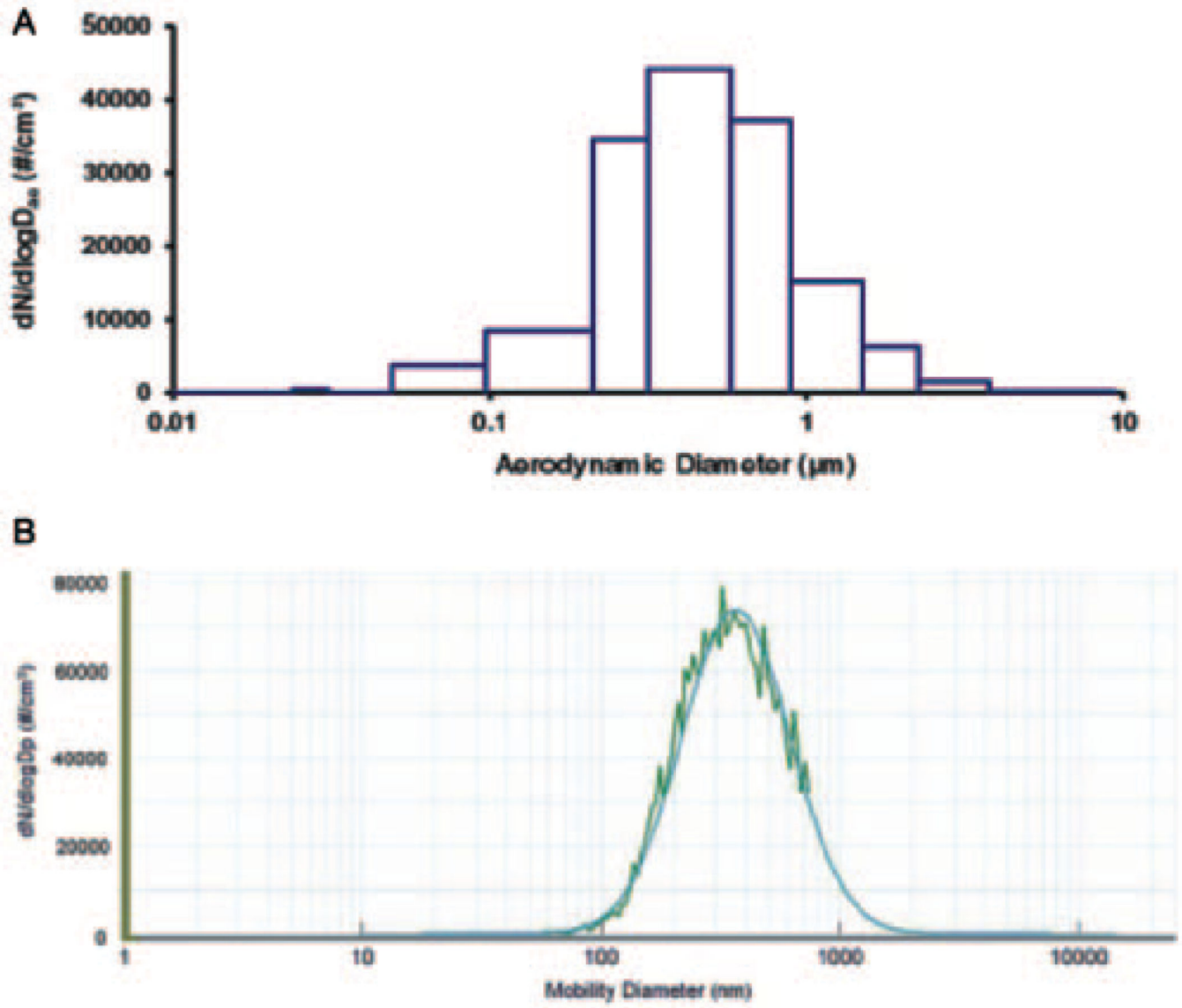

Figure 8.

Representative number-based particle size distributions of the MWCNT aerosol obtained from two near-real-time instruments. (A) A histogram obtained from ELPI, with a count median of 0.45 μm (GSD = 2.09) and a number concentration of 3.4×10^4 particles/cm^3, where N = number concentration and D_{ae} = aerodynamic diameter. (B) A zigzag curve obtained from SMPS, where D_p is the electrical mobility equivalent diameter. The smooth curve in (B) was compiled by assuming that the particle size follows a unimodal lognormal distribution. The count median is 360 nm with a geometric standard deviation of 1.70. The number concentration is 4.2×10^4 particles/cm^3.

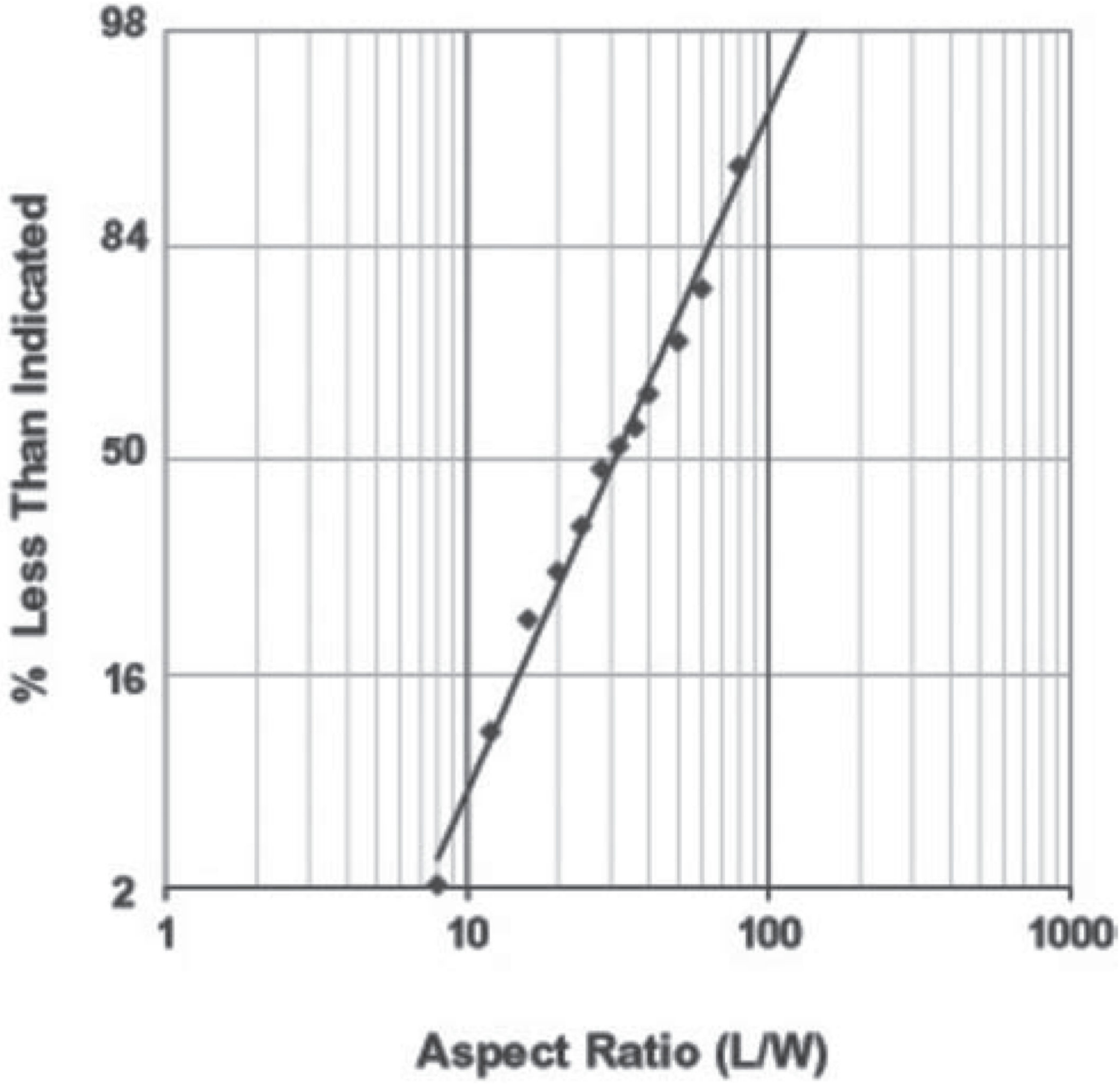

Figure 9.
Cumulative distribution of the aspect ratio of the fiberlike particles shown with a log probability plot. The count median aspect ratio and geometric standard deviation are determined as 31.0 and 2.09, respectively.

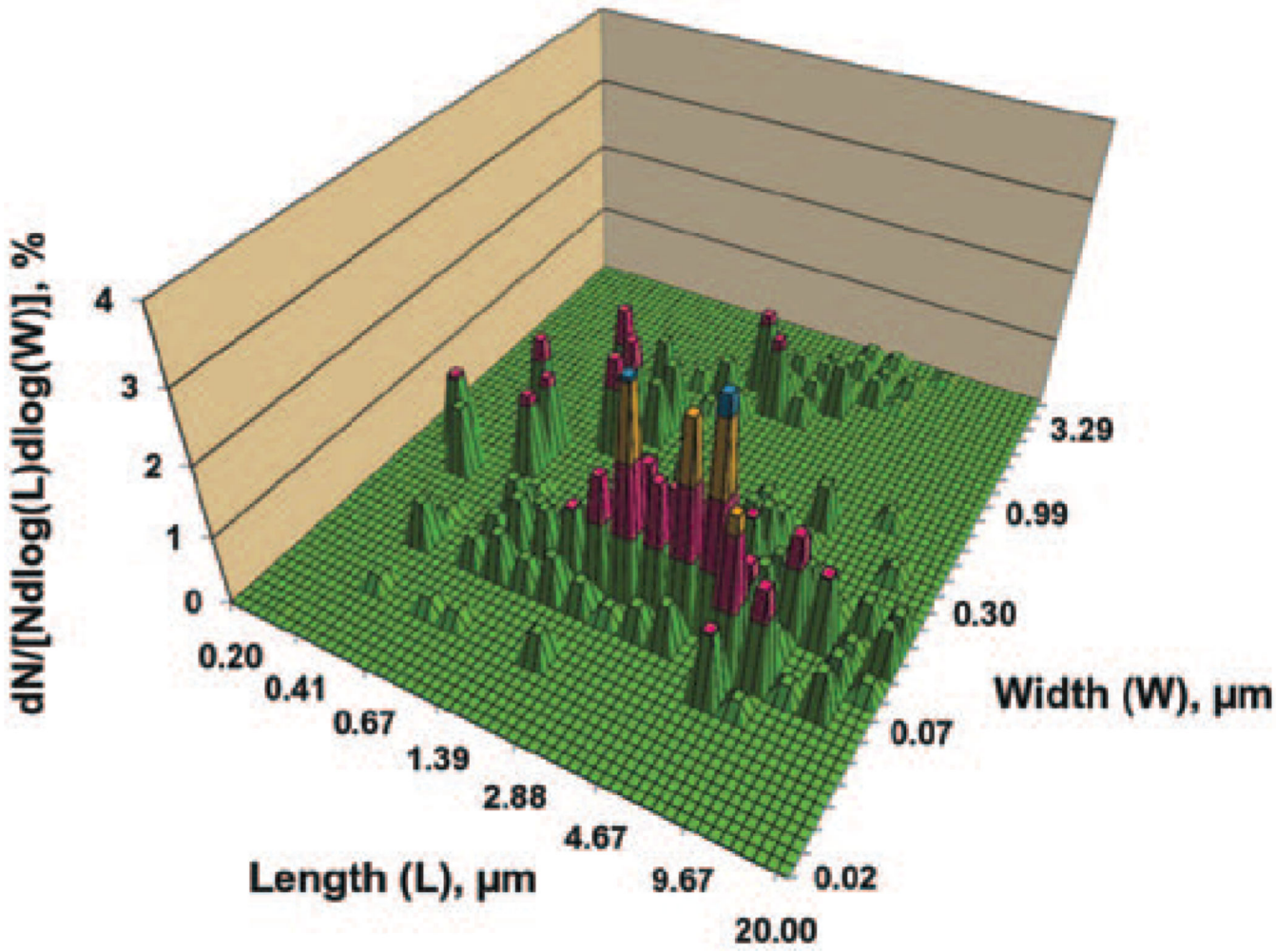

Figure 10.

The number-based size distribution of overall particles in the MWCNT aerosol collected from the animal exposure chamber. The histogram shows the percent number concentration per unit length and unit width interval (*N* = number concentration, *L* = length, and *W* = width). Different colors represent different z-values (ranging from 0 to 4 in an increment of 1). For the isometric particles (at the upper left corner of the diagram) their lengths are similar to their widths with an aspect ratio <3, whereas the aspect ratios are ≥3 for the fibrous particles (at the lower portion of the diagram). The overall distribution cannot be described by a lognormal distribution.

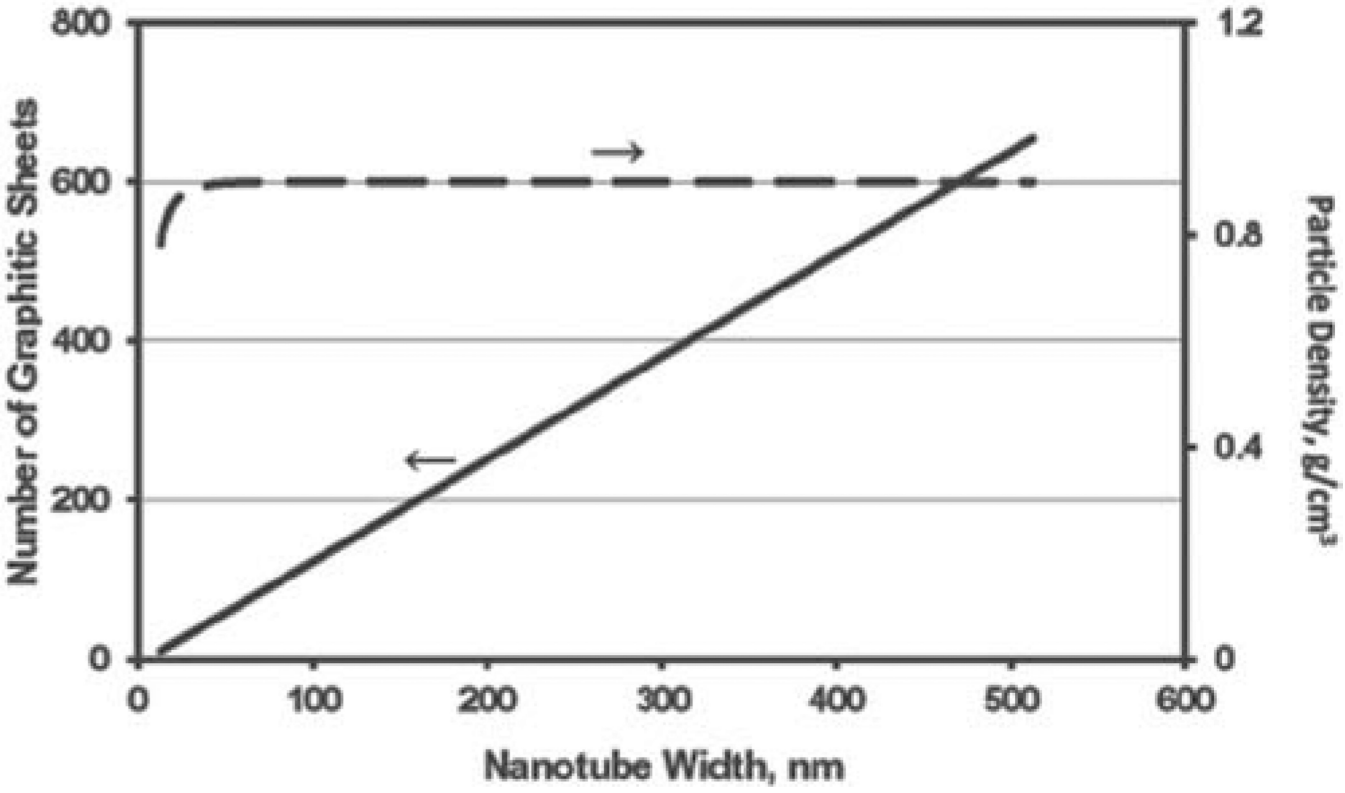

Figure 11.

The relationship of number of sheets and fiber density (with voids) of a multi-walled nanotube with respect to its tube width. The values of number of sheets and particle density were calculated based on the measurements of the nanotube from a high-resolution TEM images (Porter et al., 2010; Figure 1), in which the width of the inner hollow core (W_C) = 5.385nm, the thickness of a graphitic sheet (W_T) = 0.166 nm, and the distance between two graphitic sheets (W_D) = 0.222 nm. The material density of graphite was provided by the manufacturer as 2.1 g/cm^3

Table 1

Variation of width distribution with change in length for fiber-like MWCNT particles collected from the animal exposure chamber.

Length range (μm)	% in each length range	% fiber-like particles with width within specific length range (nm)											
		<10	10–20	20–40	40–60	60–80	80–100	100–120	120–150	150–200	200–250	250–300	300–700
<0.2	0.0												
0.2–0.4	0.4		100										
0.4–0.6	1.9			20	60	20							
0.6–0.8	3.5			11	22	22		33	11				
0.8–1.0	3.9			10	30	20	20	20					
1.0–2.0	20.5			4	15	36	19	13	6	8			
2.0–4.0	27.5				7	15	25	24	10	10	3	4	1
4.0–6.0	24.4				8	24	14	17	6	13	10	2	6
6.0–8.0	7.8				5	15	20	10	35	10	5		
8.0–10.0	3.1					13		13		50	13		13
10.0–15.0	4.3					9	18	27	18	9	9		9
15.0–20.0	2.7							14		43	29		14

Table 2

Physical characteristics of the MWCNT particles collected on the MOUDI cascade impactor: the projected area diameter, d_{pa}, and particle density, ρ_p, for the well-defined isometric particles; the length, L; width, W; dynamic shape factor, κ and aspect ratio, β; for the well-defined fiber-like particles, d_i = 50% cutoff diameter, d_{50}, on i-th stage of the impactor; N_p, number of particles measured and SD, standard deviation. On stages 1–5, 12–14 and the backup filter, there were not sufficient isometric and well-defined particles to be included in this calculation.

Impactor Stage		Isometric particles					Fiber-like particles										
			d_{pa}(μm)		ρ_p (g/cm^3)[a]			L(μm)		W(nm)		κb		β		κ[c]	
No.	d_i(μm)	Np	mean	SD	mean	SD	Np	mean	SD	mean	SD	mean	SD	mean	range	mean	SD
6th	1.0	25	1.46	0.42	0.85	0.27	32	6.38	2.58	206	69	<1	-	48.7	8.0–125.4	1.94	0.46
7th	0.56	25	0.79	0.22	0.88	0.22	37	5.46	3.15	168	47	1.20	0.44	41.9	4.0–132.5	2.10	0.67
8th	0.32	44	0.63	0.27	0.76	0.48	47	3.78	2.24	118	42	1.50	0.33	43.9	4.0–140.5	2.09	0.67
9th	0.18	31	0.27	0.08	0.85	0.26	69	2.73	2.10	83	37	2.01	0.38	40.1	4.6–198.6	2.01	0.66
10th	0.10	17	0.19	0.06	0.73	0.26	39	2.45	1.46	69	23	2.21	0.56	31.0	9.1–111.1	2.24	0.62
11th	0.06	4	0.15	0.04	0.50[d]	0.16	25	1.38	0.94	52	6	2.50	0.64	28.0	5.8–56.3	2.71	0.93

[a] Calculated from Eq (1).

[b] Calculated from Eq (3) where $d_{ae} = (d_{i-1} \times d_i)^{1/2}$ and d_i = 50% cutoff diameter on i-th stage.

[c] Calculated from Eq (4).

[d] If $d_{ae} = d_{i-1}$ =0.1 μm, then ρ_p = 0.71 g/cm^3.

Table 3

Comparison between MWCNT characterization results obtained from gravimetric and microscopic methods and two near-real-time instruments. (ELPI = electrical low pressure impactor; SMPS = scanning mobility particle sizer).

Physical characteristics	Gravimetric/ microscopic methods	ELPI	SMPS
Particle size distribution			
Count mode	0.42 μm	0.43 μm	0.35 μm
Mass mode	1.3 μm	1.84 μm	1.1 μm
MMAD/GSD	1.5 μm/1.67[a]	≈ 2.0 μm	NA
Number concentration	2.7×10^4 particles/cm^3	3.4×10^4 particles/cm^3	4.2×10^4 particles/cm^3
Mass concentration	10 mg/m^3	≈ 20 mg/m^3	3.2 mg/m^3

[a] Based on the primary mode of the size distribution.

NA, not available.